Variability Analysis in Surface Electromyography Features

by

Yiyang Shi

BEng (Hons), University of Liverpool & Xi'an Jiaotong-Liverpool University, 2013

A Thesis Submitted in Partial Fulfillment
of the Requirements for the degree of

Master of Science in Engineering

In the Graduate Academic Unit of Electrical and Computer Engineering

Supervisor(s):	Dawn MacIsaac, PhD, Electrical and Computer Eng.
	Phil Parker, PhD, Electrical and Computer Eng.
Examining Board:	Julian Meng, PhD, Electrical and Computer Eng., Chair
	Mary E Kaye, PhD, Electrical and Computer Eng.
	Erik Scheme, PhD, Electrical and Computer Eng.
	Usha Kuruganti, PhD, Kinesiology

This thesis is accepted by the
Dean of Graduate Studies

THE UNIVERSITY OF NEW BRUNSWICK

December, 2019

ABSTRACT

SEMG applications use features extracted from surface electromyography (SEMG) data as inputs. The features often exhibit high variability across subjects, activities, and even across segments from a single contraction. The purpose of this work was to provide insights into SEMG feature variability to enable better data collection and interpretation.

Variability in mean frequency (MF) and mean absolute value (MAV) was measured in simulation across stationary segments to estimate baseline variability. Then variability in the features was measured during two *in vivo* protocols involving static contractions: a single contraction 'within-trial' test and a set of contractions yielding a 'between-trial' test. For the 'within-trial' test, variability in MAV increased significantly from baseline, while the variability of MF did not (ANOVA, α=0.05, $p<0.001$, $p=0.35$, respectively). For the 'between-trial' test, variability in MAV increased further, and MF significantly increased as well (ANOVA, α=0.05, $p<0.05$, $p<0.01$). A sensitivity analysis conducted in simulation was used to infer sources for variability beyond the baseline, and the number of active motor units emerged as the likely source for 'within-trial' increases, while conduction velocity and fibre depth emerged as likely contributors to 'between-trial' increases, along with the number of active motor units.

Feature variability can also be affected by electrode position during measurement. Focusing on spectral energy, bandwidth characteristics, and signal amplitude characteristics, five features were examined for use as an index to avoid the effects of innervation zone and tendon regions. Band power ratio (BRP), MF and absolute area of a normalized action potential (AANAP) demonstrated promising results by correctly identifying >80% of poorly positioned electrode channels.

ACKNOWLEDGEMENTS

I would first like to acknowledge my best gratitude to Dr. Dawn MacIsaac and Dr. Philip Parker who have offered me this wonderful opportunity of conducting research in biomedical engineering with their knowledgeable guidance and immense patience. I could never have experienced academic research and learned about its importance, intricacies and procedures without my supervisors. Appreciations to my colleague Shriram Tallam Puranam Raghu for his helpful tips on MATLAB, data analysis and more.

Sincere appreciations to my supervisor at Carleton University – Dr. Adrian Chan – who provided me with the co-op opportunity and guidance that lead to my research topic and yielded a major part of this thesis. It was a pleasure to work under his supervision and I have fond memories of working with his other students.

Big thanks to the technicians from both ECE and IBME tech shops for providing me the material, space and guidance for preparing the equipment used in data collection. Also, this work could not have been done without the subjects who flexed their biceps to complete the work. Thank you all for your time and patience.

Lastly and most importantly, I want to thank my parents, Xin Shi and Liuqiong Liu. Without their continuous emotional, mental and financial support, I could not have completed my study.

Table of Contents

List of Tables

List of Figures

List of Symbols and Abbreviations

List of Abbreviations

AANAP	Absolute Area of a Normalized Action Potential
AMUP	Average Motor Unit Potential
ANOVA	Analysis of Variance
ARM	Autoregressive Model
BPR	Band Power Ratio
CoV	Coefficient of Variation
CV	Conduction Velocity
DAQ	Data Acquisition Device
HQ	High Quality
IEMG	Integrated EMG
ICC	Intra-class Correlation Coefficient
IP	Innervation Point of Motor Neuron
IPI	Inter-pulse Interval
IZ	Innervation Zone
KUR	Kurtosis
LQ	Low Quality
MAV	Mean Absolute Value
MDF	Median Frequency
MF	Mean Frequency
MU	Motor Unit
MUAP	Motor Unit Action Potential
MUAPT	Motor Unit Action Potential Train

MVC	Maximum Voluntary Contraction
NBW	Normalized Bandwidth
NMU	Number of Motor Units
NSM	Normalized Spectral Moments
PSD	Power Spectral Density
RMS	Root-mean-square
SD	Standard Deviation
SEMG	Surface Electromyography
SFAP	Single Fibre Action Potential
SSC	Slope Sign Change
WAMP	Willison Amplitude
WL	Waveform Length
ZC	Zero Crossing

List of Symbols

f_{c}	Cut-off Frequency
f_{s}	Sampling Frequency
B_{S}	Statistical Equivalent Bandwidth
M	Number of Samples in a Power Spectral Density
m	Frequency-domain Sample Index
N	Number of Samples in a Signal
n	Time-domain Sample Index
N_{R}	Number of Segments
p	P-value of Statistical Analysis

T	Signal Length in Time
T_{R}	Segment Length in Time
T_{s}	Sampling Interval in Time
T_{w}	Window Length in Time
α	Significance Level of Statistical Analysis
μ	Mean
σ	Standard Deviation
σ^2	Variance
$\Phi_{xx}(f)$	Power Spectral Density

CHAPTER 1 INTRODUCTION

1.1 Objectives

Surface Electromyography (SEMG) is a non-invasive technique used for detecting the electrical activity produced when muscles are activated. It provides information about activation patterns, levels of muscle contraction, and other muscular states, which can be used to drive a variety of SEMG-based applications, for instance gesture control devices (Du, et al., 2017) or diagnostic tools such as the Nicolet EDX® system(Natus Medical, Inc., ©2016). Despite its potential, SEMG is difficult to measure robustly (Balshaw, et al., 2017), and difficult to interpret (Farina, et al., 2004).

Taking consistent SEMG measurements is difficult to do because they are affected by a variety of factors including an individual's physiological characteristics, the muscular activities engaged in during measurement, the sensors (electrodes) and instrumentation technologies used to construct the measurement system, and set-up details like where the sensors are positioned. Each of these factors can influence features extracted from SEMG data which are used as inputs to drive SEMG-based applications. They add to the baseline variability in feature estimates, which is always present due to the random nature of SEMG signal generation. Insight into what contributes to variability in feature estimates can help guide improved measurement and analysis in SEMG-based applications, so the primary goal of this work was to examine feature variability in order to contribute to our understanding of it.

In the first component of the work reported here, variability in mean absolute value (MAV) and mean frequency (MF) estimates was investigated, because these are two

commonly used features in SEMG-based applications. For instance, MAV is used widely in myoelectric control devices (Englehart & Hudgins, 2003; Oskoei & Hu, 2008; Al-Angari, et al., 2016), and MF is a common feature used in SEMG-based fatigue analysis (Phinyomark, et al., 2012; Marco, et al., 2017). Variability in these features was investigated via simulation to ascertain a baseline for what to expect as a minimum level resulting from sampling error, and to examine possible sources of additional variability as they are introduced during contractions, such as changes in muscle geometry, recruitment of additional fibres with increasing strength of contraction etc. Findings from simulation were then compared to variability observed in data recorded during *in vivo* experimentations, with attempts made to explain variability using knowledge gleaned from the simulation analysis. In summary, the objectives of this component of the work were:

- Objective 1: to use simulated SEMG to establish a baseline variability for features based on variability due to sampling error.
- Objective 2: to determine the influence on feature estimates, of physiological parameters associated with the generation of SEMG signals, through a sensitivity analysis conducted via simulation.
- Objective 3: to compare simulation results with *in vivo* experimentation to infer what might be changing during contraction so that it may be considered during measurement and analysis.

During the simulation analysis, electrode placement along the muscle was found to affect SEMG signal feature values considerably, especially when placed near innervation zones

(IZs), where nerve initiates muscular contraction, or near tendon regions, where muscles attach to bone. This is consistent with what is reported in literature (Merletti, et al., 2001; Rainoldi, et al., 2004). Electrode placement is therefore an important consideration when trying to measure SEMG signals consistently.

Although the effect of electrode placement can be minimized by collecting multiple channel locations using linear electrode arrays and selecting the least-affected channel, these kinds of measurements add to the complexity of SEMG collection and processing, so single-channel SEMG is still commonly used (Gazzoni, et al., 2016; Merlo & Campanini, 2016). Example applications include biofeedback (Sturma, et al., 2018), sport science (Hug & Tucker, 2017) and diagnosis of neuromuscular conditions (Naik, et al., 2016). Since there is no existing technique for identifying locations affected by IZ or tendon regions with single-channel SEMG, guidelines based on geometrical landmarks observable from human bodies such as the SENIAM recommendations (Hermens & Freriks, 1997) are typically used to avoid these regions during measurement. However, the locations of IZ and tendon can vary considerably (Piccoli, et al., 2014) so that following the SENIAM recommendations does not always lead to avoiding placement over IZ and tendon.

In the second component of this work, SEMG feature sensitivity to electrode location was examined in an effort to identify a feature which could be used as an index to discern electrode locations affected by IZ and tendon regions with single-channel SEMG. This was done with data recorded during *in vivo* experimentation with an electrode array of 7 channels spread along the muscle. The objective of this work was specifically:

- Objective 4: to extract feature values from SEMG data measured at electrode locations spread from close to far proximity with respect to innervation zones and tendon regions in order to identify any features that clearly separate data affected by these regions from data that are not.

The two components of this work as outlined above are described in detail in Chapters 2 and 3 respectively, which contain verbatim journal articles currently submitted for publication. Both articles have been submitted to the Journal of Electromyography and Kinesiology, a leading publication in the field of EMG studies. The author of this thesis is the principal author of both articles. Thesis supervisors are co-authors on both articles and Dr. Adrian Chan, a professor in the Department of Systems and Computer Engineering at Carlton University, is also co-author of the second article. He supervised the experimental data collection for that study and contributed guidance through analysis. For a summary of results and contributions from these papers, refer to the concluding Chapter 4. The rest of this chapter provides an overview of the major concepts used and discussed in the articles.

1.2 Overview of SEMG Simulation, Feature Estimation and Feature Variability

1.2-1 MyoSim V2.0 – an SEMG Simulation Tool

An SEMG signal is obtained as the measured electrical activity of muscles at the surface of skin. The fundamental component of a skeletal muscle is the motor unit (MU) which contains a motor neuron and all the muscle fibres it innervates. A muscle contraction is achieved by the simultaneous and consecutive activation of motor units. Upon the activation of a motor neuron, all the fibres in its MU will be activated, causing a potential

change around each fibre that can be detected by sensors at the skin surface nearby. The potential detected from a single fibre is called the single fibre action potential (SFAP) while the potential from all fibres from a MU is called the motor unit action potential (MUAP). During a muscle contraction, the recruited motor units are activated at some rate described by firing statistics, resulting in a train of MUAPs separated by an inter-pulse interval (IPI). The summation of motor unit action potential trains (MUAPTs) from all MUs activated during the contraction is an SEMG signal.

In this work, the simulation tool MyoSim V2.0, originally developed by MacIsaac et al. (2006) and recently updated by MacIsaac et al. (2018) was used to simulate SEMG signals. MyoSim uses a finite-length model originally proposed by Plonsey (1974) and further developed by Gonzalez-Cueto and Parker (2002). With this model, SFAPs measured at the skin surface are generated by convolving a bi-directional propagating differential source with a tissue filter dependent on fibre parameters including: fibre conduction velocity, depth of the fibre, and location of innervation point relative to electrodes and the ends of the fibre. The MUAPs measured at the skin surface are then generated by summing the SFAPs of the corresponding MU. MUAPTs are formed by convolving MUAPs with impulse trains representing the innervation process with specified IPI (or firing statistics). Finally, a simulated SEMG signal is generated by summing all the individual MUAPTs from all the activated MUs. This process is depicted in Figure 1-1.

The fibre geometry used in the generation of MUAP with MyoSim is depicted in Figure 1-2. Each fibre within an MU has distinct geometry, modelled as uniform dispersions around centre values.

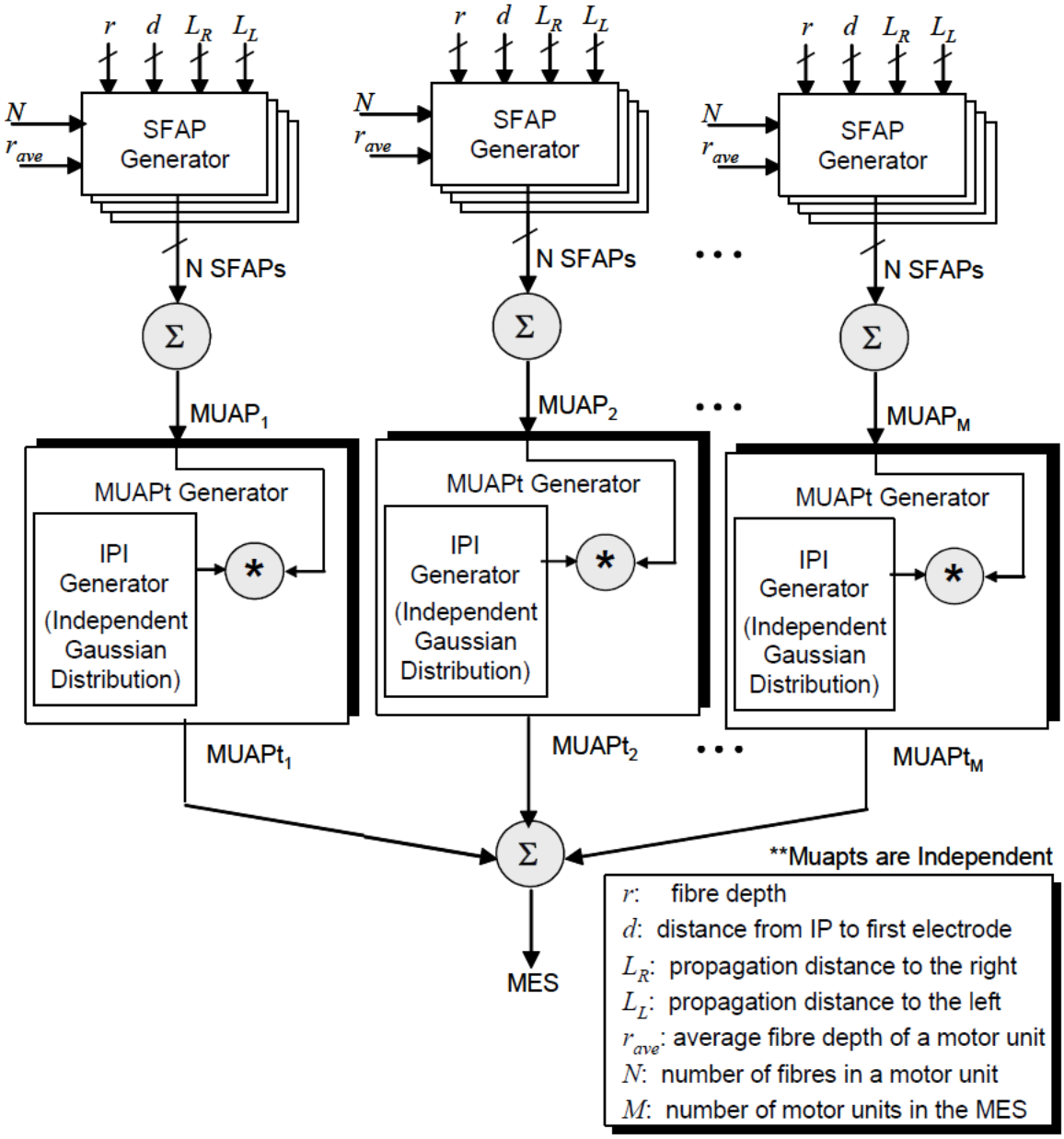

Figure 1-1: Summary of the EMG modelling process (MacIsaac, 2004)

Example waveforms of simulated SFAP, MUAP, MUAPT and SEMG waveforms are depicted in Figure 1-3, extracted from a simulated bipolar SEMG recording with 58 MUs. The figure shows the MUAP and MUAPT from a MU that contains 331 fibres, with conduction velocities ranging from 3.9-4.3m/s, proximal terminations set at

180±5mm from innervation point (IP), distal terminations set at 220±5 from IP, and IPIs ranging from 33.4-45.2ms. Electrode locations are modelled to be 50mm and 60mm from the IP, and fibre depths are set to 8.2±5mm from the electrodes. The SFAP shown in this figure (Figure 1-3a) has a depth of 4.95mm, a conduction velocity of 3.99m/s, a proximal termination 176.4mm and a distal termination 215.3mm. Table 1-1 delineates the parameters set in MyoSim to generate this example.

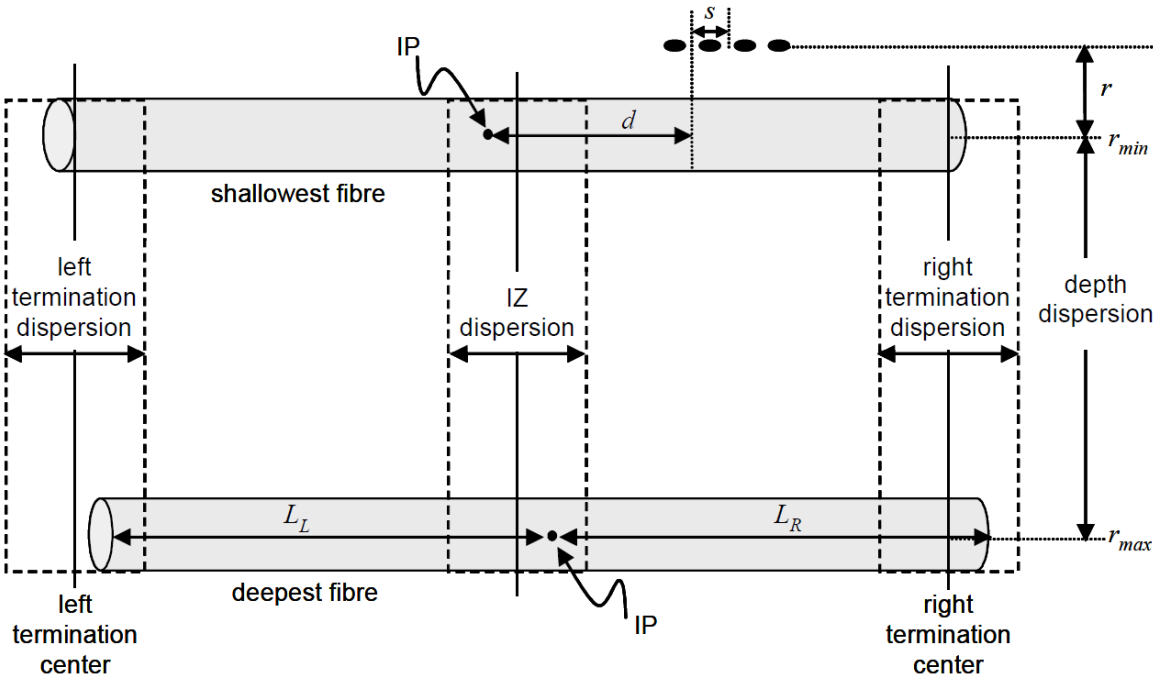

Figure 1-2: MUAP model parameters (IP: motor neuron innervation point; d: distance between electrode and IP; s: electrode spacing; r: fibre depth; L_L: distance between IP and distal termination; L_R: distance between IP and proximal termination). (MacIsaac, 2004)

Parameters	Value	Parameters	Value
Fibres per Motor Unit	331	Number of Motor Units	58
Distal Termination	-220 ± 5 mm*	Motor Unit Depth	6.1~22.1 mm**
Proximal Termination	180 ± 5 mm*	Motor Unit Alignment	−20~20 mm**
Radius of Motor Units	5 mm	Radius of Limb	40 mm
Inter-pulse Interval	33~100ms***	Electrode Locations	$50, 60 \pm 5$ mm****
Conduction Velocity	4.1 ± 0.2m/s*	Electrode Configuration	Single Differential

*Uniform random dispersion across fibres; ** Uniform random dispersion centred at 14.1mm in depth and 0mm in alignment; ***Uniform random dispersion across motor units; ****Distance measured with respect to innervation points. Dispersion indicated is across innervation points of different fibres.

Table 1-1: MyoSim parameter values for the simulated recording shown in Figure 1-3.

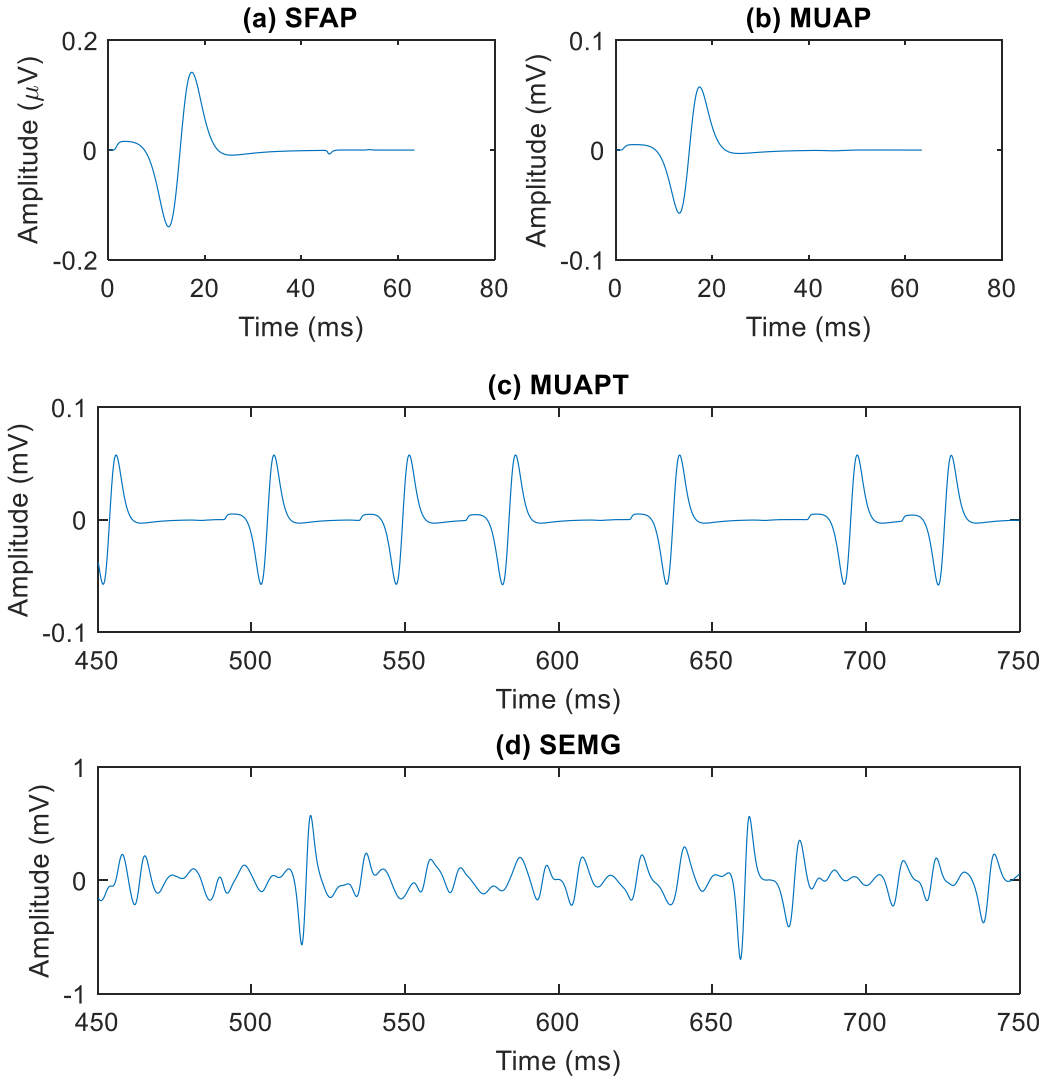

Figure 1-3: a) SFAP, b) MUAP, c) MUAPT and d) SEMG waveforms from a simulated recording generated by MyoSim V4.5. The MUAP waveform is the sum of its 331 fibres, the MUAPT has an IPI of 33.4-45.2ms while the SEMG waveform is the sum of 58 MUAPTs.

Enhancements to MyoSim were made for the current work in order to conduct the simulation analysis. The enhancements were made so that MyoSim could reload SFAP, MUAP and MUAPT parameters and waveforms generated in a previous session, to simulate a new recording with a subset of the parameters originally used. Figure 1-4 depicts a screen shot of the window for setting parameters while simulating based on previously specified parameters.

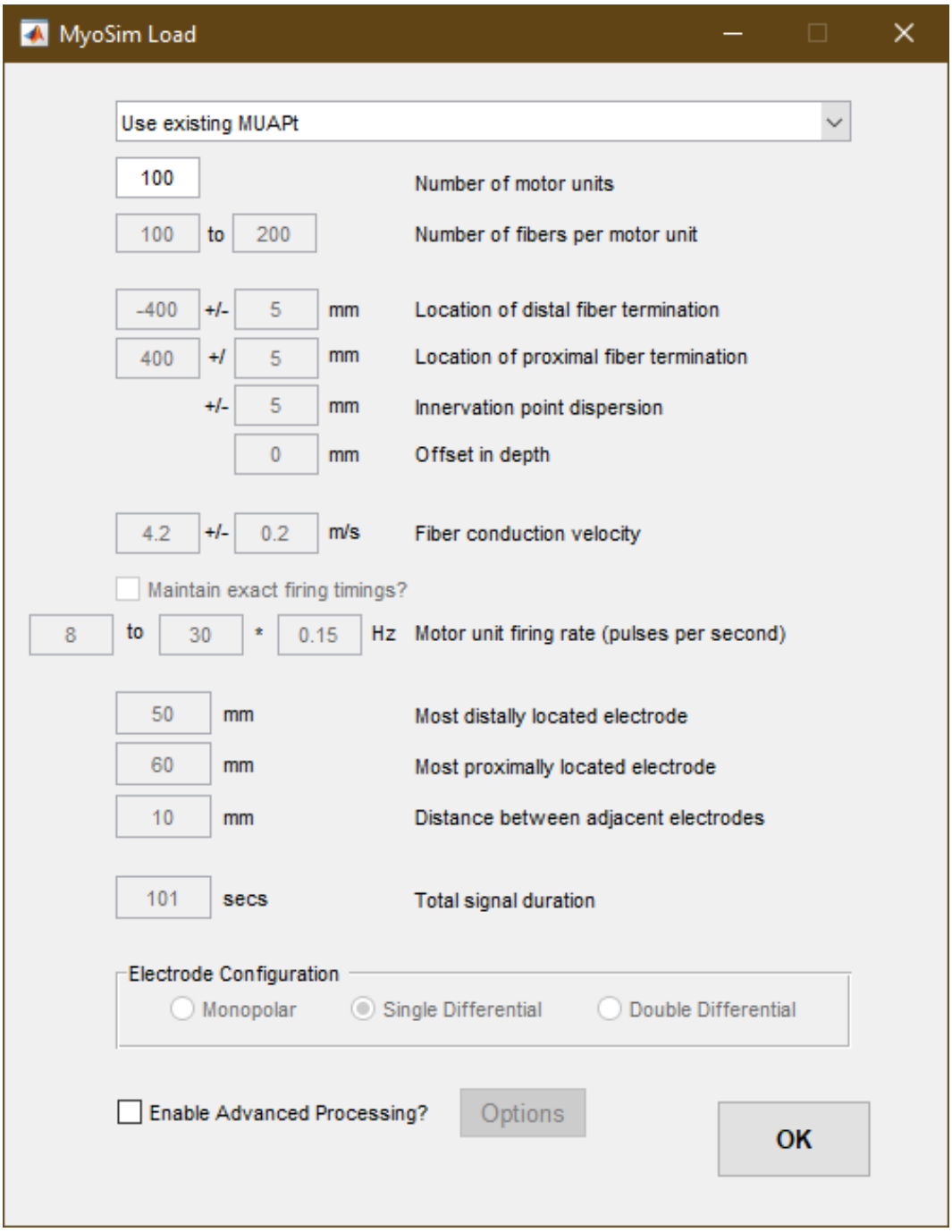

Figure 1-4: Screenshot of MyoSim parameters window when simulating based on a loaded signal.

1.2-2 SEMG Features Estimation

In SEMG applications, a variety of features that represent different aspects of SEMG signal characteristics are used. For example, Hudgins & Parker (1993) proposed a time-domain feature set that is commonly used in myoelectric control (Scheme & Englehart,

2014; Smith, et al., 2010). For a sampled and quantized SEMG recording $x[n]$ containing N samples, these features are described below in Table 1-2. A MATLAB library for computing these features was used in this work, as provided by Chan (2018).

Feature Name	Description	Equation
Mean Absolute Value (MAV)	The mean of the rectified SEMG signal.	$MAV = \frac{1}{N}\sum_{n=1}^{N}\|x[n]\|$
Zero Crossings (ZC)	The number of sign changes within a signal. A threshold Th is set to ignore crossings caused by noise.	$ZC = \sum_{n=1}^{N-1} f(x[n] \times x[n+1]) + \sum_{n=1}^{N-1} g\left(\frac{x[n+1]}{x[n]}\right)$ $f(x) = \begin{cases}1, x \leq Th \\ 0, x > Th\end{cases}$ $g(x) = \begin{cases}1, x = 0 \\ 0, x \neq 0\end{cases}$
Slope Sign Change (SSC)	The number of slope sign changes within a signal. A threshold Th is set to ignore changes caused by noise.	$SSC = \sum_{n=2}^{N-1} f\big((x[n] - x[n-1]) \times (x[n+1] - x[n])\big)$ $f(x) = \begin{cases}1, x \leq Th \\ 0, x > Th\end{cases}$
Waveform Length (WL)	The cumulative length of the signal.	$WL = \sum_{n=1}^{N-1}\|x[n+1] - x[n]\|$

Table 1-2: Commonly used time-domain features for myoelectric control.

Features that describe the frequency-domain characteristics of an SEMG signal have been reported extensively in tracking muscle fatigue, as delineated by Arjunan et al. (2014). Such features include mean frequency, median frequency and normalized spectral moments. For a power spectral density (PSD) estimate $\Phi_{xx}(f)$ with M samples, these features are described in Table 1-3. The expressions used to calculate the features have been taken from Rogers & MacIsaac (2013).

Feature Name	Description	Equation
Mean Frequency (MF)	The estimated "centre of mass" for a PSD estimate.	$MF = \frac{\sum_{m=1}^{M} f_m \Phi_{xx}(f_m)}{\sum_{m=1}^{M} \Phi_{xx}(f_m)}$
Median Frequency (MDF)	The frequency which divides the PSD estimate into two regions with equal area.	$MDF = f_K$ such that $\sum_{m=1}^{K} \Phi_{xx}(f_m) = \sum_{m=K}^{M} \Phi_{xx}(f_m)$
Normalized Spectral Moments (NSM)	A generalized form of MF to the k^{th} order.	$NSM_k = \frac{\sum_{m=1}^{M} f_m^{-1} \Phi_{xx}(f_m)}{\sum_{m=1}^{M} f_m^{k} \Phi_{xx}(f_m)}$

Table 1-3: Frequency-domain features commonly used for muscle fatigue studies.

In fatigue studies, the observed changes in the above frequency-domain features can be attributed to the spectral shifts caused by changing conduction velocity (CV) (De Luca, 1984). The most common way to estimate CV is to measure the delay between two signals measured a known distance apart along the propagation direction of the muscle. For two signals collected at channel locations along a muscle separated by distance d, the peak of their cross-correlation will be located at delay Δt, and CV can be obtained as:

$$CV = \frac{d}{\Delta t} \qquad \text{1-1}$$

Obviously, estimating CV in this way requires the collection of two channels. The technique is sensitive to small differences in channel characteristics, and perturbations in channel alignment with muscle fibres. Thus, CV is a feature that is not widely used in SEMG-based clinical and commercial applications. However, CV estimates often demonstrate abnormal values near innervation zones and tendon regions (Merletti, et al., 2003), making it useful in identifying these regions for research purposes.

In addition to the features described in Table 1-2 and Table 1-3, SEMG signal quality analysis has focused on features described in Table 1-4.

Feature Name	Description	Equation
Four-term autoregressive model (ARM) coefficients	The ARM computes the N^{th} sample of a signal x as a linear combination of the previous 4 samples. Each of the coefficients $a_1, a_2, \dots, a_K$ that minimize the squared error between $x[n]$ and $\hat{x}[n]$ for all n are used as a feature.	$\hat{x}[n] = \sum_{i=1}^{4} a_i x[n-i] + w_n$
Ten-bin Histogram	The number of samples in each bin from a 10-bin histogram of a SEMG signal with equal bin widths. The number for each bin is used as a feature.	/
Ten-bin Averaged PSD	The PSD is computed by using Fast Fourier Transform and then squaring the result. This PSD is divided into 10 frequency bins with the mean of each bin's spectrum value used as a feature.	/
Willison Amplitude (WAMP)	The number of times the absolute difference between adjacent samples exceed a predetermined threshold Th.	$WAMP = \sum_{n=1}^{N-1} h(\lvert x[n+1] - x[n] \rvert)$ $h(x) = \begin{cases} 1, x \geq Th \\ 0, x < Th \end{cases}$

Table 1-4: Additional features used in SEMG signal quality analysis.

Other interesting features also reported in the literature include: band power ratio (BPR), used in diaphragmatic fatigue studies (Gross, et al., 1979) and myoelectric control (Oskoei & Hu, 2008); kurtosis (KUR), used in characterizing the probability distribution of SEMG signals (Nazarpour, et al., 2013); average motor unit potential (AMUP), whose characteristics was studied for the estimation of recruitment pattern (Komi & Viitasalo, 1976); and bandwidth (BW), which is used to track muscle fatigue (Rogers & MacIsaac, 2011). For a SEMG signal $x[n]$ with N samples and its PSD estimate as $\Phi_{xx}(f)$ with M samples, these features are described in Table 1-5.

Feature Name	Description	Equation
Band Power Ratio (BPR)	The power ratio between two frequency bands $[f_{1,lo}\ f_{1,hi}]$ and $[f_{2,lo}\ f_{2,hi}]$.	$MF = \frac{\sum_{f=f_{1,lo}}^{f_{1,hi}} \Phi_{xx}(f)}{\sum_{f=f_{2,lo}}^{f_{2,hi}} \Phi_{xx}(f)}$
Kurtosis (KUR)	For a distribution described by a random variable x with mean μ and variance σ^2, kurtosis reflects its flatness and tendency to have outliers. $\mathrm{E}(\cdot)$ represents the expectation operator.	$KUR = \frac{\mathrm{E}[(x-\mu)^4]}{\sigma^4}$
Average Motor Unit Potential (AMUP)	For a SEMG signal $x(t)$ normalized by its maximum value $x_{\max}$, a list of spike locations $T_{\mathrm{sp}}[i]$ of length N_{sp} is first determined by finding the locations of local maximums that are above half the maximum amplitude of the signal, with spikes spaced at least 0.01s from each other. The ensemble average is then taken across samples from 0.01s before to 0.01s after each spike.	$AMUP(t) = \frac{1}{N_{\mathrm{sp}}} \sum_{i=1}^{N_{\mathrm{sp}}} \frac{x\left(T_{\mathrm{sp}}[i]+t\right)}{x_{\max}}$ $t \in [-0.01, 0.01]$ second
Bandwidth (BW)	The difference between upper corner frequency $f_{c,hi}$ and lower corner frequency $f_{c,lo}$. Corner frequencies are defined as the frequencies at which the power drop to half of the peak in a PSD.	$BW = f_{c,hi} - f_{c,lo}$

Table 1-5: Features used in establishing an index for the quality of electrode location.

While the first part of the current work focused on examining variability in MAV and MF, the second part investigated MF, BPR, KUR (on the shape of PSD), the area of absolute AMUP and normalized BW in the search for an electrode site quality index.

1.2-3 SEMG Feature Variability

Factors that are sources of SEMG feature variability can be categorized as internal or external factors. External factors are factors that can be readily controlled during measurement, such as the muscles and tasks involved, measurement set-ups, and feature estimation techniques. Conversely, internal factors, mostly physiological parameters such as motor unit recruitment patterns (combinations of activated MUs) and muscle geometry

(fibre length, IZ location etc.), cannot be directly controlled during measurement. The categories, relationships and lists of factors are delineated in Figure 1-5.

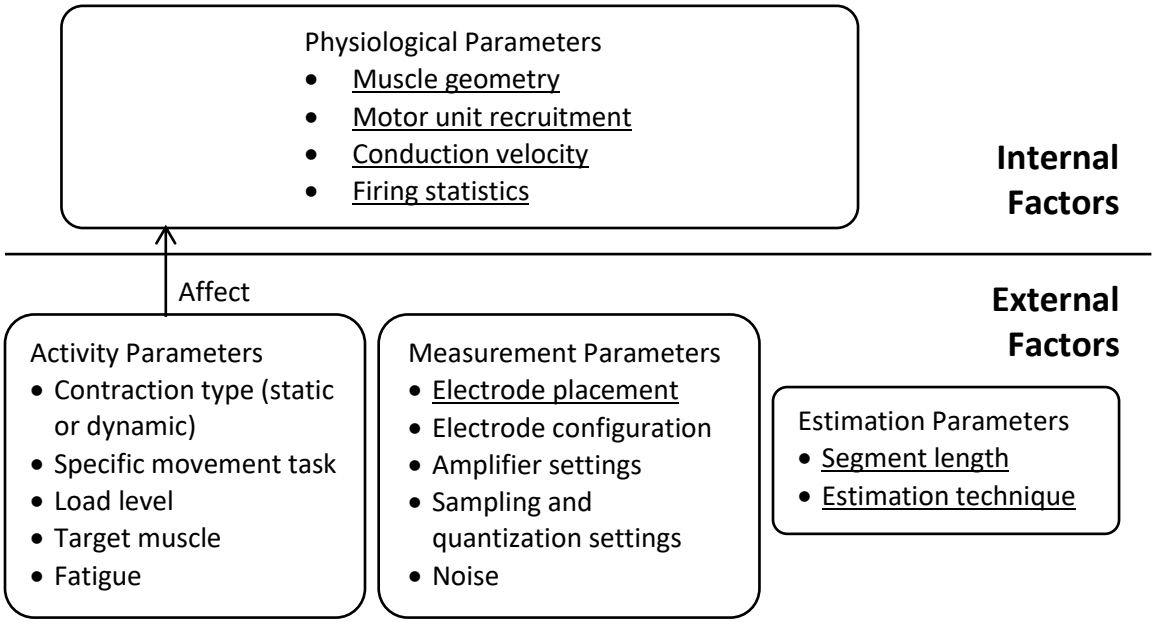

Figure 1-5: Categories, relationships and list of parameters that are sources of SEMG feature variability, with factors investigated in this work underlined.

Sources of variability that the current work focused on are underlined in Figure 1-5. They are mostly internal factors. Firing statistics is of particular interest, because it is a random process which results in variability from segment to segment during the course of a measurement, even when all other factors are held constant. It is therefore the source of variability due to sampling error which cannot be avoided during measurement. Measurements on one individual and a specific muscle under static conditions (isometric/isotonic) provide limited control over the other internal factors, which are strongly influenced by activity parameters. However, even static contractions can introduce variability due to internal factors, based on changes in recruitment, which can lead to changes in all of the other internal factors based on which MUs are active. Insights into how all of these sources contribute to the additional variability observed

within well-controlled single isometric/isotonic contractions and between such contractions are provided in this work.

Existing work reports on variability of SEMG features under various conditions, in efforts to quantify the limits of repeatability (Zaman, 2012; Carius, et al., 2015; Sorbie, et al., 2018). The most commonly tested features include amplitude features such as root-mean-square (RMS) value and Integrated EMG (IEMG) and central frequency features such as median or mean frequency (MDF/MF). Mixed results have been reported on feature repeatability. For example, the RMS value across isometric maximum voluntary contractions performed in a single session was reported to be reliable for the pericranial muscle (Jensen, et al., 1993b), while high variability was reported for the tibialis anterior muscle (Araujo, et al., 2000). MDF slope over time is used as a fatigue measure during isometric contractions. Its between-session reliability was reported as extremely unreliable for the quadriceps muscle (McCarthy, et al., 2008), while demonstrated good reliability for the paraspinal muscle at most recording sites (Ebenbichler, et al., 2002).

Much of the existing work reports on the effect of external factors, but little work has been reported on internal factors, likely because they are hard to study *in vivo*. Arnall et al. (2002) report that a load level of 50% maximum voluntary contraction is the most reliable level when assessing muscle fatigue using initial MDF, slope of MDF and slope of RMS. Similar results were reported by Rainoldi et al. (1999), who observed highest repeatability at a load level of 50% MVC for initial MNF and initial MAV during sustained static contractions. The same study also reported smaller within-day and between-day variability in initial MDF for the bicep brachii muscle compared to the findings of Ng and Richardson (1996) for back muscles. Such dependency of

repeatability on the analyzed muscles was also observed by Karamanidis et al. (2002). The study found higher repeatability in MF for gastrocnemius lateralis (GL) and gastrocnemius medialis (GM) than tibialis anterior (TA), vastus lateralis (VL) and hamstrings (HA), and higher repeatability in IEMG for GM, GL, TA and HA muscles than VL, during running cycles with different velocities and stride frequencies. In addition to load level and target muscle, Kollmitzer et al. (1999) found that the intra-subject variance of MF and RMS estimates from upper leg muscles during isometric contractions at MVC and 50% MVC increased as the interval between contractions increase from 3 minutes to 90 minutes. Baratta et al. (1998) discussed the sources of variability in MF estimates, and proposed three methods for reducing the variability in PSD, a major source of MF variability.

The first component of the current work focuses on the effects of internal factors, which has been rarely discussed in the literature. Conversely, the effect of electrode placement on SEMG feature estimates has been confirmed in many studies. In particular, these studies report that placing electrodes near innervation zones or tendon regions will result in variations in MAV, MF, MDF and CV estimates (Roy, et al., 1986; Jensen, et al., 1993a). An informative discussion of the effect is provided by Merletti et al. (2001). Additional variance in feature estimates can also be introduced due to inconsistent electrode placements between test sessions or electrode shift during a test session (e,g, dynamic contractions). To avoid electrode sites that are affected by such effect, the use of multi-channel SEMG is currently required. Attempts to find an index that identifies affected locations using single-channel SEMG were made in the second component of this work.

CHAPTER 2 WITHIN-TRIAL AND BETWEEN-TRIAL VARIABILITY IN SURFACE EMG FEATURES

2.1 Introduction

The use of surface electromyography (SEMG) is promising in a wide range of applications such as assistive device control (Scheme & Englehart, 2011), muscle condition assessment during ergonomic and sport science studies (Rainoldi, et al., 2000), diagnosis of neuromuscular and musculoskeletal disorders (Rainoldi, et al., 2004), and rehabilitation (Shenoy, 2010). While it can provide insight into underlying neuromuscular processes, SEMG can be difficult to interpret, which in part, is due to variability in SEMG data (Farina, et al., 2004; Merletti, et al., 1999; Merletti, et al., 2001; Huckabee, et al., 2012). Characteristic features extracted from SEMG signals can demonstrate high variability between individuals, test protocols, testing sessions, and even between trials collected from the same individual during a single session (Rainoldi, et al., 1999). This leads to difficulties in reliable interpretation and application of results.

Variability in SEMG features has been measured and reported extensively in the literature in efforts to quantify the limits of repeatability. Carius et al. (2015) provide an excellent summary of studies on intrasession variability which evaluate variability across trials within a same-day session. Other studies provide a look into between-day (or intersession) variability with the intent to rationalize mean power frequency as a repeatable measure for muscle fatigue (Rainoldi, et al., 1999; Arnall, et al., 2002; Mathur, et al., 2005). Most of the cited studies focus on amplitude features such as root-mean-square (RMS) value or Integrated EMG (IEMG), and some also report on central frequency features such as median or mean power frequency (MF). Collectively these

studies yield mixed results regarding the repeatability of RMS value, IEMG and MF, which is not surprising given the diversity of muscles, activities, experimental set-ups, and estimation procedures utilized in the studies.

Variability in SEMG features stems from many sources. Physiological parameters that influence signal features include which motor units are active, the number of fibres associated with each active unit, the geometry of each fibre with respect to the measuring electrodes (including fibre length, depth, location of innervation point, and the relative position to each other), the conduction velocity of each fibre, and random firing patterns (i.e. interpulse intervals) of each motor unit. These parameters are subject dependent, introducing variability across subjects. They are also activity dependent, influenced by factors such as the length of contraction, the type of contraction (e.g. static vs. dynamic), and the level of contraction (weak or strong). This dependence introduces variability across activities. Also, parameters associated with the measurement set-up itself can influence SEMG features. Such parameters include electrode configuration (monopolar vs bipolar), electrode spacing, and electrode positioning, as well as amplifier bandwidth, noise, and sampling and quantization settings.

Subject and activity dependent physiology can be controlled by taking measurements from a single subject engaged in a particular activity, while measurement parameters can be controlled using a single measurement setup. Even then, variability will manifest within and between trials. Physiological parameters may change from contraction to contraction, and even over the course of a single contraction as different motor units are recruited and firing patterns are augmented. Also, the random nature of firing statistics makes the signal random. Features can only be estimated from a measured sample and

are subject to the effects associated with sampling error. It is therefore necessary to use statistical inference when interpreting SEMG data, even when interpulse interval between motor unit action potentials is the only source of variability.

Typically, studies on SEMG feature variability report in terms of coefficient of variation (CoV), and/or intra-class correlation coefficient (ICC). Both of these metrics are related to the standard deviation across measured samples. The CoV is simply a ratio between the standard deviation of a feature estimate and its mean. It can be estimated across measurements from a single cluster (e.g. a set of MF values measured from an individual), but because it reflects a variability measure which is relative to the mean of the data, it allows for comparisons across clusters with different means (e.g. sets of MF values from many individuals). ICC must be measured across multiple clusters. There are different ways to estimate ICC (for a thorough review, see McGraw and Wong (1996) or Shrout and Fleiss (1979)) but all represent an estimate of the fraction of the total variance that is due to variation between the clusters. Since the total variance includes both within and between-cluster variance, ICC reflects a ratio between these sources of variability. When the ICC is high, the within-cluster variance is small, relative to the between cluster variance. This generally indicates that the measured values within each cluster (e.g. MF values from each individual) are sufficiently similar to each other so that different clusters can be easily distinguished. In this work, since clusters are made up of measurements from each individual, and it is already known SEMG features are subject dependent, the variability between clusters is not of interest. Thus, variability is reported using CoV, which is calculated as

$$CoV = \frac{\sigma}{\mu} \quad \text{2-1}$$

where σ and μ is the standard deviation and mean across feature estimates respectively.

The purpose of this work was to investigate variability in SEMG feature measurements to ascertain an expected minimum level and examine possible sources of additional variability as they are introduced across trials. It is problematic to isolate the sources of variability using SEMG data recorded *in vivo*, because physiological parameters cannot be readily controlled or directly measured during *in vivo* experimentation. Because of this, an SEMG simulation tool was first used to establish expected contributions of different variability sources. Statistical and sensitivity analyses were conducted on MF and Mean Absolute Value (MAV) estimates from simulated signals. Then these expectations were compared to variability observed in data recorded during *in vivo* intrasession experimentation. The more that is known about how sources of variability influence SEMG feature estimates, the better these sources can be attended to during experimental design, data collection, feature estimation and interpretation.

2.2 Methods

Simulation and experimentation were combined to investigate variability in MF and MAV feature values extracted from SEMG segments. First, an analysis was conducted on simulated data to determine the expected variability in feature value estimates arising solely from stationary firing statistics and finite segment length. Since this is the minimal, unavoidable variability, it is referred to here as 'baseline variability'. Then an analysis was conducted on simulated data to estimate the expected sensitivity of feature values to changes in physiological parameters including average fibre depth, conduction velocity

and number of active motor units. Finally, *in vivo* experimental data was recorded from the bicep brachii on the dominant arm of 11 subjects (7 male and 4 female, average age of 24.4±3.17) to estimate within-trial and between-trial variability in MF and MAV. Each subject completed all trials at two contraction levels. For each contraction level, a 15-second contraction was collected from each subject to estimate within-trial variability and 15 5-second contractions were collected to estimate between-trial variability.

2.2-1 Simulated Data

To perform a variability analysis on controlled SEMG signals, the simulation tool MyoSim V4.5, originally developed by MacIsaac et al. (2006) and updated by MacIsaac et al. (2018), was used for signal generation. MyoSim simulates SEMG signals based on a finite-length model of muscle fibres which was developed by Gonzalez-Cueto and Parker (2002). Single fibre action potentials (SFAPs) measured at skin surface are generated by convolving a bi-directional propagating double layer differential source and a tissue filter dependent on fibre conduction velocity and fibre geometry (length, depth and location of innervation point relative to electrodes) (Plonsey, 1974). Then motor unit action potentials (MUAPs) measured at the skin surface are generated by summing multiple SFAPs with user specified physiological parameter values (i.e. those listed above along with the number of fibres per motor unit). Finally, MUAP trains are formed by convolving MUAPs with impulse trains representing the innervation process with user specified firing rates. By summing the individual MUAP trains, a simulated SEMG signal is generated. The number of motor units firing is also user configurable.

The signals in this work were simulated to represent a single differential (bipolar) electrode configuration placed about 30mm proximal to the innervation zone of the

biceps muscle. Table 2-1 delineates user specified parameters available in the MyoSim tool. Values in the table reflect those found in typical bicep brachii as indicated in the literature (Lee, et al., 2008; Wheeler, et al., 2010) and by experience, and were used as reference values. Simulated records were generated based on the reference values, and were used for two analyses: first to determine baseline variability, and then to conduct a sensitivity analysis.

Parameters	Value	Parameters	Value
Fibres per Motor Unit	$300{\sim}400^{***}$	Number of Motor Units	100
Distal Termination	-180 ± 5 mm*	Motor Unit Depth	$12{\sim}30$ mm**
Proximal Termination	160 ± 5 mm*	Motor Unit Alignment	$-15{\sim}15$ mm**
Radius of Motor Units	5 mm	Radius of Limb	40 mm
Firing Rate	$10{\sim}30$Hz***	Electrode Locations	$30, 40 \pm 5$ mm****
Conduction Velocity	5 ± 0.2m/s*	Electrode Configuration	Single Differential

*Uniform random dispersion across fibres; ** Uniform random dispersion centred at 21mm in depth and 0mm in alignment; ***Uniform random dispersion across motor units; ****Distance measured with respect to innervation points. Dispersion indicated is across innervation points of different fibres.

Table 2-1: List of MyoSim parameters with reference values for bicep brachii.

2.2-1a Determining Baseline Variability

Statistical sampling variability in SEMG features refers to the variability across feature value estimates due to finite duration sample records and random firing intervals. It is the theoretical minimum variability in a feature estimate given a stationary random generation process. In simulation, this stationarity condition can be easily met, and such a process, if observed over infinite time, would yield a feature value estimate equal to the true value. However, even in simulation, feature values must be estimated from finite-length segments and sampling errors arise leading to baseline variability between estimates. The magnitude of sampling error is related to the segment length observed and estimation technique applied (e.g. how power spectrum is estimated to calculate the MF feature). The estimation technique was held constant for this work simply by using a consistent technique, but segment length was investigated.

To establish baseline variability for different segment lengths, 100 contiguous segments were extracted from one long stationary signal simulated with duration $T = 3000\text{s}$ and sampling frequency $f_s = 5000\text{Hz}$. Muscle parameters were set to the reference values delineated in Table 2-1 and MF and MAV values were calculated for each segment according to Equation 2-2 and 2-3 respectively. This process was repeated for segment lengths from $T_R = 1$ s to $T_R = 30$ s, by extracting the first $N_R = T_R \cdot f_s$ data points from each segment. The mean and standard deviation across segments were reported for each feature and segment length.

For an SEMG segment X, MF was calculated according to:

$$MF_X = \frac{\sum_{m=1}^{M} f_m \Phi_{xx}(f_m)}{\sum_{m=1}^{M} \Phi_{xx}(f_m)} \quad \textbf{2-2}$$

where M is the length of the power spectral density (PSD), f_m is the frequency of the m^{th} component in the PSD and $\Phi_{xx}(f_m)$ is the magnitude of PSD at frequency f_m. The PSD estimates were calculated using the squared magnitudes of the Fast Fourier Transform (FFT) coefficients of the segment, without any averaging.

MAV was calculated according to:

$$MAV_X = \frac{\sum_{n=1}^{N_R} |x_n|}{N_R} \quad \textbf{2-3}$$

where x_n is the n^{th} data point of X.

Both MF and MAV are known to be affected by one or more of the physiological parameters defined in the simulation model. Thus, the results provided through the processing outlined above apply only to a signal matching the reference values. To make a comparison between simulated baseline variability and variability in signals recorded through *in vivo* measurement, effort was made to produce a set of simulated signals that

remained stationary, but otherwise matched the records. A matching strategy recently developed by Tallam Puranam Raghu (2017) was used to accomplish this. This strategy employed a genetic algorithm to optimize simulation input parameters so that the simulation output would match a particular signal. The algorithm uses a comparison of PSD estimates from the simulated and recorded data as its fitness function. The number of motor units, number of fibres per unit, fiber depth, and conduction velocity were optimized. Each within-trial record was matched yielding a set of 22 simulated signals with the kind of variability in physiological parameters expected for 11 subjects each engaging in contractions at two different force levels. Each of these signals was simulated with duration $T = 100\text{s}$ and sampling frequency $f_s = 5000\text{Hz}$ and the signals were segmented into 100 1-second segments. MF and MAV were calculated for each segment and the mean, standard deviations and coefficients of variation were reported for each feature.

Records collected from electrodes in single differential configuration during isometric/isotopic and non-fatiguing contractions, as simulated here, can be properly described as a stationary random process with Gaussian distribution and zero-mean (Clancy, 1999). As a result, the MAV estimate for a segment extracted from an SEMG record is the mean of a folded symmetric Gaussian distribution. The CoV of MAV estimates across segments from an SEMG record X described by such a process can be obtained as (Parker, et al., 1977)

$$\text{CoV}[MAV_X] \approx \frac{1}{\sqrt{4B_\text{S}T_\text{R}}} \qquad \textbf{2-4}$$

where T_R is the length of each segment in seconds and B_S is the statistical equivalent bandwidth in Hz given by

$$B_S = \frac{[\sum_{m=1}^{M} \Phi_{xx}(f_m)]^2}{\sum_{m=1}^{M} \Phi_{xx}^2(f_m)} \quad \text{2-5}$$

where M is the length of the PSD of X, f_m is the frequency of the m^{th} component in the PSD and $\Phi_{xx}(f_m)$ is the magnitude of PSD at frequency f_m. This value can be considered to be the theoretical CoV and hence baseline value for an SEMG record under the stationary Gaussian assumptions.

Since T was fixed at 1s for the simulation, CoV of MAV estimates across segments is determined solely by B_S. Since B_S can be calculated from the PSD estimate of any signal, its corresponding CoV value can also be obtained using Equation 2-4. Theoretical values for the CoV of MAV were calculated and reported along with the values calculated based on the mean and standard deviation across segments.

2.2-1b Sensitivity Analysis

To determine the influence of changing physiological parameters on MF and MAV estimates, a sensitivity analysis was performed on simulated signals. By changing the values of one parameter while leaving the others constant, effects from the changing parameter were isolated. Starting with the reference values for parameters delineated in Table 2-1, each parameter was varied in isolation within a range identified as reasonable for bicep brachii contractions.

Preliminary analysis was conducted on a variety of simulation parameters to eliminate parameters yielding negligible effects. Average fibre depth, conduction velocity, and motor unit recruitment emerged as influencing factors. To observe the sensitivity to each of these factors, a signal was generated with the reference parameters and then regenerated identically (i.e. with the same motor units), except for a set of values

incrementally altered for each of the parameters of interest. This yielded a set of signals that included the reference signal plus one for each of the altered values. All of these signals were generated with a duration of $T = 100\text{s}$, and segmented into 100 segments, for MF and MAV to be calculated. The means across segments were then plotted against the changing parameter so that sensitivity, defined as the absolute value of the rate of change in feature per unit change in parameter, could be ascertained from tangent slopes in the curves.

To observe sensitivity to fibre depth, each fibre was moved from its reference location in increments of 2 mm. Since all fibres were moved by the same amount each increment, these shifts are reported here as shifts from the average depth across all fibres. The average depth for the reference signal was 21 mm. The average depth for the regenerated signals was varied from 17 mm to 29 mm.

In MyoSim, each fibre's conduction velocity is set by dispersing a value around an average velocity. The reference values for these parameters were set to 5±0.2 m/s. To observe sensitivity to CV, the average velocity was varied in increments of 0.5 m/s from 3.5 m/s to 6.5 m/s. The dispersion value was not varied.

The reference value for the number of motor units was set to 100. To simulate a variation in motor unit recruitment, signals were generated from subsets of the reference motor unit action potential trains originally generated. The number of motor units in each subset was varied in increments of 2 from 2 to 10, then in increments of 5 from 15-50, and finally in increments of 10 from 60 to 90. Ten different combinations of motor units were used in each of the 17 cases generated in addition to the reference signal.

2.2-2 Recorded Data

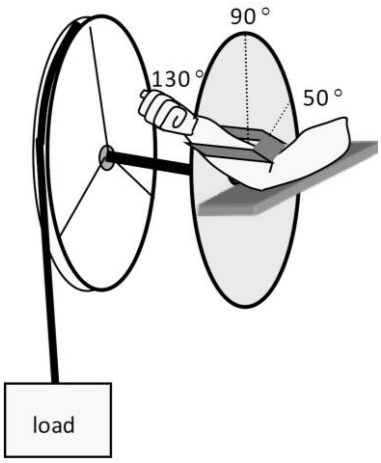

Figure 2-1: The disk-pulley apparatus used for loading the bicep brachii.

A disk-pulley apparatus (as shown in Figure 2-1) was used to load the bicep brachii muscle isometrically and isotonically during within- and between-trial tests. For each of the 11 subjects, all of the tests were performed in the same session so experimental set-up, including electrode placement, remained constant. The target skin surface was cleaned with rubbing alcohol before 5 Ag-AgCl bar electrodes (size 6×1mm, 5mm spacing) were placed near the muscle belly, where each electrode was perpendicular to the muscle. SEMG data were recorded using these electrodes in single differential configurations which resulted in 4 channels per record. To avoid signals with electrode placement issues (near the innervation zone or tendon regions), only one channel was chosen for analysis. Channels yielding CV estimates outside the range of 3.2-7.2 m/s or with unusual power spectra shape based on visual inspection were discarded. This sometimes resulted in more than one valid channel. When more than one channel for a subject was deemed valid, the channel with minimum MF was chosen for analysis since MF increases with proximity to innervation zone and tendon regions (Merletti, et al., 2003; Farina, et al., 2004b).

SEMG signals from electrodes were processed first through a pre-amp configuration described previously by Lovely (1993), and then through Tektronix AM502 amplifiers. The combined gains were set between 4000 and 10000, depending on subject, and the low and high cut-off frequencies of these amplifiers were set to 10Hz and 1000Hz respectively. From the amplifier, the signal was connected to an oscilloscope for display,

and through an anti-aliasing filter (cut-off frequency, $f_c = 500\text{Hz}$). The signals were sampled at $f_s = 5000\text{Hz}$ and quantized with 16-bit resolution by a Measurement Computing™ PCIM-DAS1602/16 board.

Both the within-trial and between-trial tests were designed with loads at 25% and 15% of the subject's maximum voluntary contraction (MVC) with elbow angle held constant at 90° for a short duration (5s and 15s respectively). Such activity yields isometric/isotonic contractions with minimum fatigue. MVC was quantified during a separate session as the maximum load a subject could lift at the elbow angle using a Free Motion F624 cable machine. Elbow angle was monitored via a potentiometer on the disk-pulley apparatus as a means of verifying the isometric contraction and quantifying angle variation. Despite it is impossible to have direct control over the physiological parameters of a muscle, the use of short static contractions helps to constrain known sources of physiological changes.

The within-trial test included 1 isometric/isotonic contraction for each load level. Each contraction was held for 15s, yielding a record that was segmented into 15 1-second segments. A rest period of 60s was enforced between contractions while subject remained in place to maintain a constant arm position. MF and MAV were estimated from each of the 1-second segments as delineated in Section 2.2-1a and CoV across estimates was calculated for each record.

During the between-trial test, subjects were asked to repeat 5s isometric/isotonic contractions 15 times with 20s of rest between contractions. As in the within-trial test, this protocol was carried out for contractions at each load level. The subject remained in place for the entire test to maintain a constant arm position. A 1-second segment was

extracted from the middle of each contraction, resulting in 15 1-second segments for processing, for each level. This data was processed identically to the within-trial test data so that variability could be compared between these conditions.

To identify any differences in variability between the three data capture protocols (i.e. simulation/within-trial/between-trial), a statistical analysis was conducted on CoV. A three-factor ANOVA was used with sex, contraction level, and data capture protocol as factors, at a significance level of α=0.05. *Post hoc* paired t-tests with Bonferroni correction were performed to ascertain the factors contributing to any significant differences indicated.

2.3 Results

2.3-1 Baseline Variability and Coefficient of Variation

Figure 2-2 depicts the mean and standard deviation of MF and MAV estimates across 100 segments versus segment length for the stationary signal simulated with the reference parameters. As expected, the baseline variabilities in both features decrease as segment length increases due to the corresponding increase in number of data points used to make the estimates. For consistency, 1-second segments were used for the remainder of the work. At 1 second, the coefficient of variation across 100 segments of this simulated signal was 3.07% for MF and 4.75% for MAV.

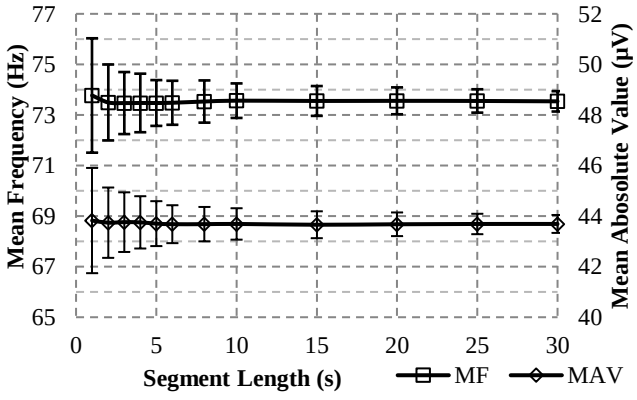

Figure 2-2: Mean and standard deviation of MF and MAV estimates across 100 segments in different segment lengths (simulated SEMG with parameters delineated in Table 2-1).

Figure 2-3a depicts MF values estimated from 100 segments for each of the simulated signals, and 15 segments for the within-trial and between-trial records. Figure 2-3b depicts the same information for MAV. These figures offer a visualization of feature variability. The simulated results represent the baseline variability expected for stationary SEMG. Within-trial results represent our best attempt to measure baseline variability during in-vivo experimentation. Between-trial results represent how variability is affected by resting and restarting. Note that joint angle in both the within-trial and between-trial tests varied less than 1 degree across segments pooled from all records for each subject. Also, MF showed no trends across records for any subject (regression analysis), indicating the absence of fatigue.

Figure 2-4 depicts the CoV of MF and MAV for each of the simulated signals and recorded data records. Note that the MAV figure also shows theoretical values based on bandwidth estimates from the simulation data. Figure 2-5 summarizes these data by depicting CoV values averaged across records, for the simulated, within-trial, and between-trial data. The boxes represent standard deviation while the whiskers show extreme values. Note that CoV values for within-trial and between-trial records were limited to 15 feature estimates due to available record lengths. This causes some increased effects from sampling error compared to the CoV values for simulated data, calculated across 100 feature estimates.

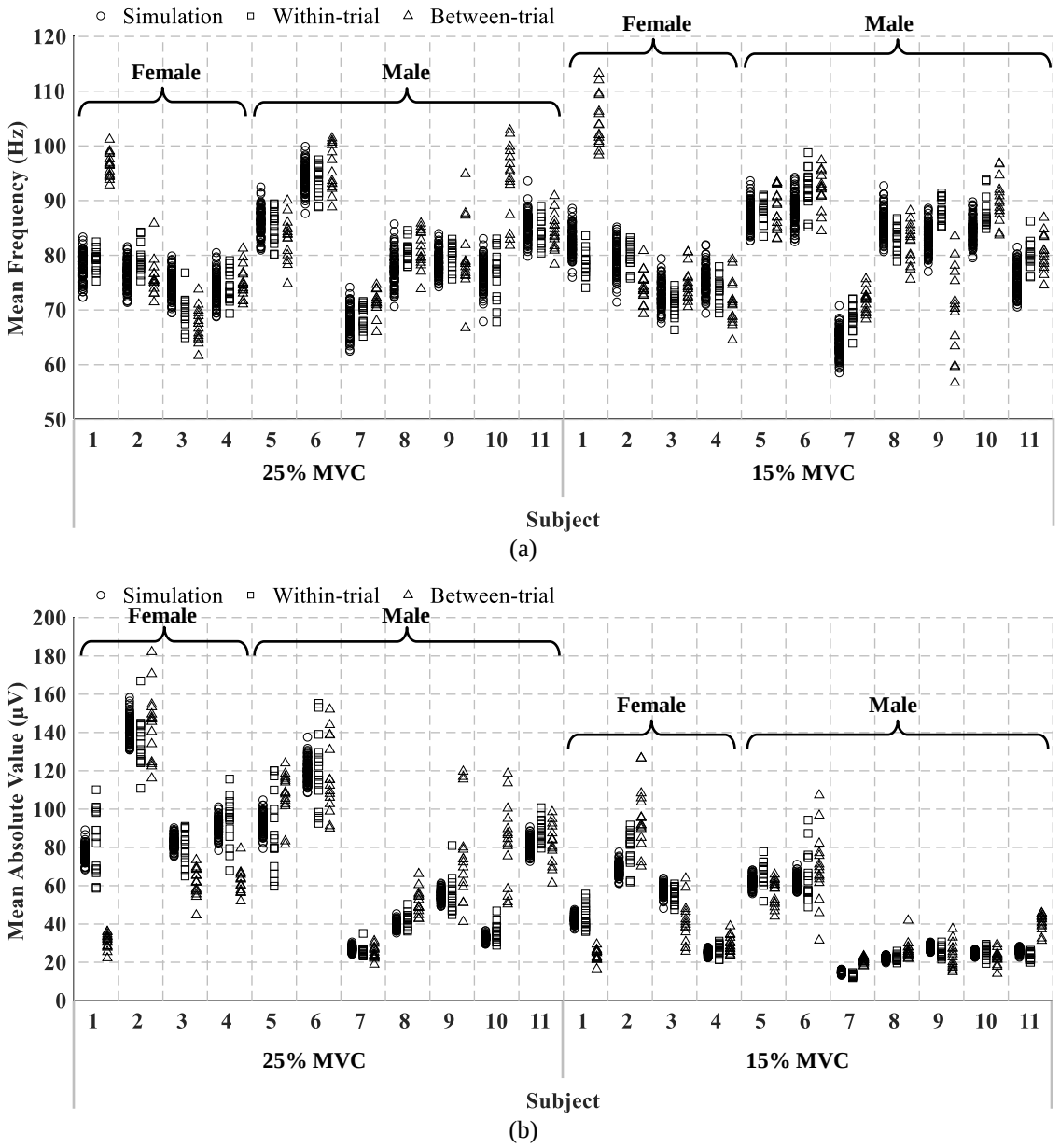

Figure 2-3: Per-segment a) MF b) MAV estimates of simulation, within-trial and between-trial records, for 11 subjects and 2 MVC levels.

The mean ± standard deviation of CoV across records are shown in Figure 2-5 which provides a means for comparing simulated signals, within-trial records, and between-trial records. For simulation data, the CoV values were $\mu \pm \sigma = 2.96 \pm 0.34\%$ for MF and 4.40 ± 0.32 for MAV. Note that the theoretical CoV values for MAV were $\mu \pm \sigma = 4.67 \pm 0.21\%$ which are comparable to simulated results. For the within-trial records, CoV

values were μ±σ = 3.18±0.81% for MF, and 12.00±4.84% for MAV. For the between-trial records, CoV values were μ±σ =4.08±0.85% for MF, and 14.83±5.69% for MAV.

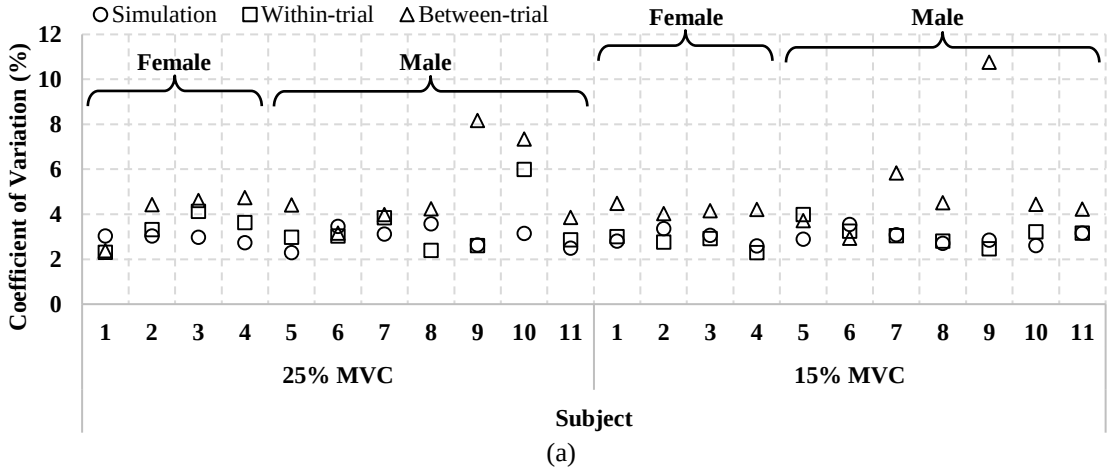

(a)

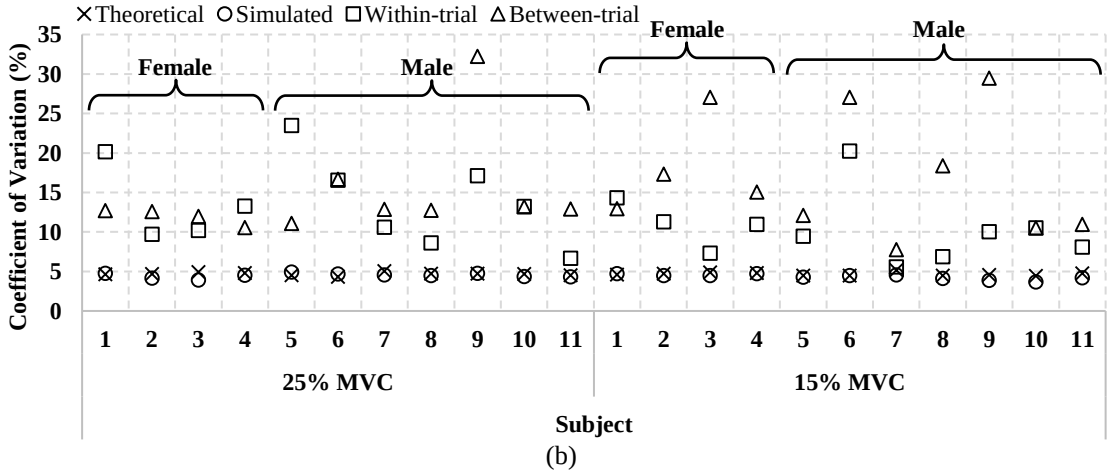

(b)

Figure 2-4: CoV of a) MF b) MAV estimates across segments for simulation, within- and between-trial records across 11 subjects and 2 MVC levels.

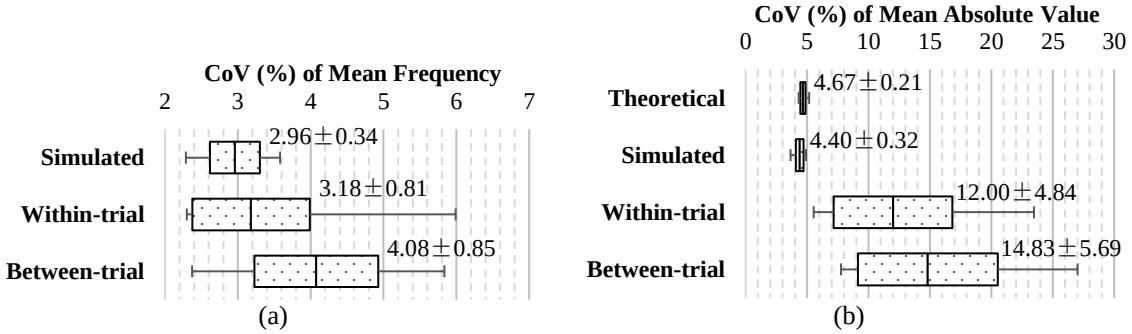

(a) (b)

Figure 2-5: Distribution of CoV values for a) MF b) MAV across 22 simulation, within-trial or between-trial records. Boxplots indicate standard deviation while whiskers indicate extreme values. Theoretical CoV values of MAV were calculated for simulation records.

Results of the statistical analysis on MF (three-factor ANOVA, $\alpha = 0.05$) indicated significant difference for data capture protocols ($p < 0.001$), but no significant difference was detected for sex ($p = 0.59$), contraction levels ($p = 0.83$) or interactions ($p > 0.35$ for all interactions). Similar results were found for MAV, where ANOVA indicated significant difference for data capture protocols ($p < 0.001$), but no significant difference was detected for sex ($p = 0.90$), contractions levels ($p = 0.94$) or interactions ($p > 0.15$ for all interactions). As revealed by the p-values from the *Post hoc* analysis shown in Table 2-2, CoV significantly differed between all data capture protocols, with the exception of simulation and within-trial data for MF.

Feature	Simulation/Within-trial	Simulation/Between-trial	Within-trial/Between-trial
MF	$p = 0.35$	$\boldsymbol{p < 0.001}$	$\boldsymbol{p = 0.0015}$
MAV	$\boldsymbol{p < 0.001}$	$\boldsymbol{p < 0.001}$	$\boldsymbol{p = 0.043}$

Table 2-2: P-values from *post hoc* paired t-tests with Bonferroni correction for the two-factor ANOVA on CoV values with MVC level and data capture protocol as factors, at a significance level of $\alpha = 0.05$ (significance shown in bold).

2.3-2 Sensitivity Analysis

Figure 2-6a depicts MF as a function of average fibre depth, for different values of CV, based on simulation. This figure illustrates that MF can be modelled as having a 3rd-order decreasing trend with depth that is scaled-up for increasing values of CV. This trend is a result of the tissue filtering effect. Given the depicted family of curves, the sensitivity of MF to changes in fibre depth decreases with increasing depth. At the reference value of 21 mm, sensitivity ranges from 4.7Hz/mm to 8.4Hz/mm for the CV values depicted.

Figure 2-6b depicts MF as a function of CV, for different average fibre depths. This figure illustrates that MF can be modelled as having an almost linearly increasing trend with CV that is scaled-down for increasing values in depth. This is likely due to the time

scaling effect in action potentials detected by single differential electrode configuration as CV changes. Given the linear relationship depicted in the figure, the sensitivity of MF to changes in CV is almost constant. At the reference value of 5m/s, sensitivity ranges from 9.5Hz/m/s to 21Hz/m/s for the fibre depths depicted.

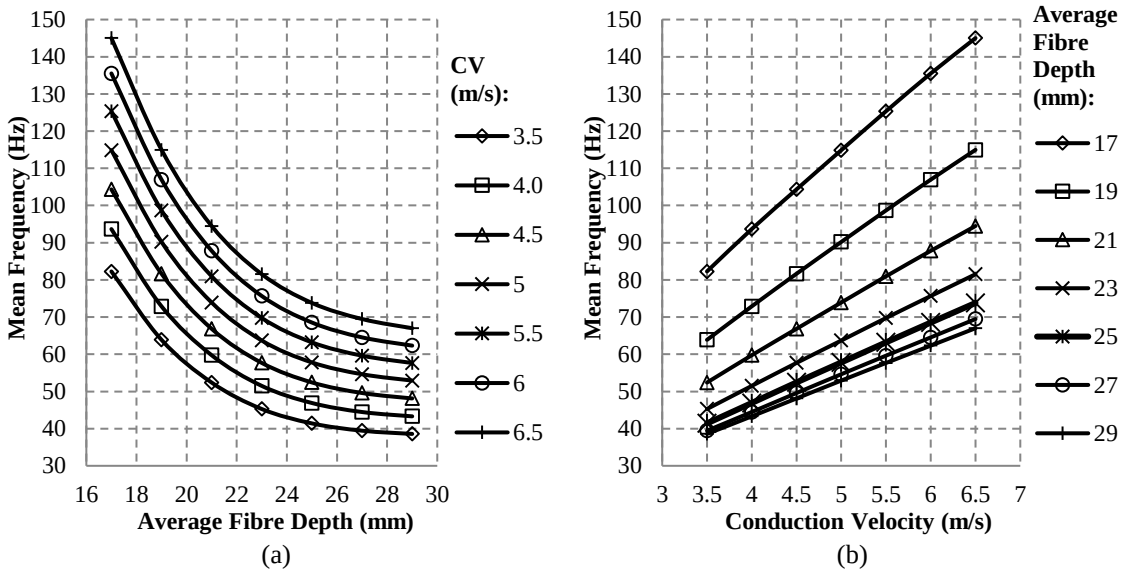

Figure 2-6: a) MF versus fibre depth for various CV; b) MF versus CV for various fibre depths (simulated SEMG).

Figure 2-7a depicts MAV as a function of average fibre depth, for different values of CV, based on simulation. The figure illustrates that MAV can be modeled as a 4th-order decreasing trend that is scaled-up for increasing values of CV. This trend is a result of the tissue filter effect. Given the depicted family of curves, the sensitivity of MAV to changes in fibre depth decreases with increasing depth. At the reference value of 21 mm, sensitivity ranges from 4.2µV/mm to 16.5µV/mm for the CV values depicted.

Figure 2-7b depicts MAV as a function of CV, for different fibre depths. The figure illustrates that MAV can be modeled as a 2nd-order increasing trend that is scaled-down for increasing values of CV. This trend is consistent with the known inverse relationship between amplitude and CV combined with the time-scaling effect of CV (González-

Cueto & Parker, 2002). Given the family of curves depicted, the sensitivity of MAV to changes in CV increases with CV. At the reference value of 5m/s, sensitivity is ranges from 6µV/m/s to 57µV/m/s for the depth values depicted.

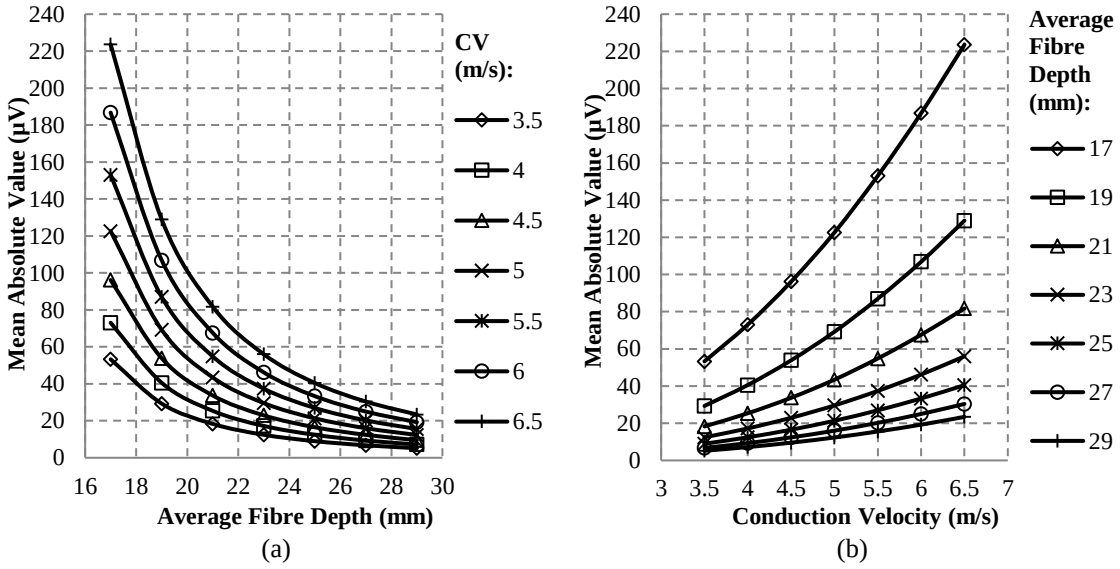

Figure 2-7: a) MAV versus fibre depth for various CV; b) MAV versus CV for various fibre depths. (simulated SEMG)

Figure 2-8 depicts MF and MAV as a function of Number of Motor Units (NMU). Ten data points for each NMU are shown, calculated from random subsets of motor units, all selected from the set of 100 units included in the reference signal, also shown on the plot. Note that any motor unit can be chosen for inclusion in more than one of the subsets. The mean across data points is shown and indicates a convergence towards constant MF for NMU>25, and an increasing trend in MAV. This trend is expected with increasing fibre activity and is well documented in the literature (Suzuki, et al., 2002; Farina, et al., 2004a; Farina, et al., 2010; Yao, et al., 2000). The trend is roughly linear and converges to a sensitivity of 0.28µV/NMU for MAV when NMU>50. Since MF converges to a constant, its sensitivity is 0Hz/NMU when NMU>25.

Figure 2-8 shows that low NMU values lead to more variability across subsets in both MF and MAV. For low NMU, each subset is more likely to be made up of a unique set of motor units, but as NMU increases, subsets begin to share units which reduces variability of feature values across the subsets. Figure 2-9 depicts CoV of MF and MAV versus NMU to capture this effect from motor unit recruitment. Note that the MAV plot also shows the theoretical values.

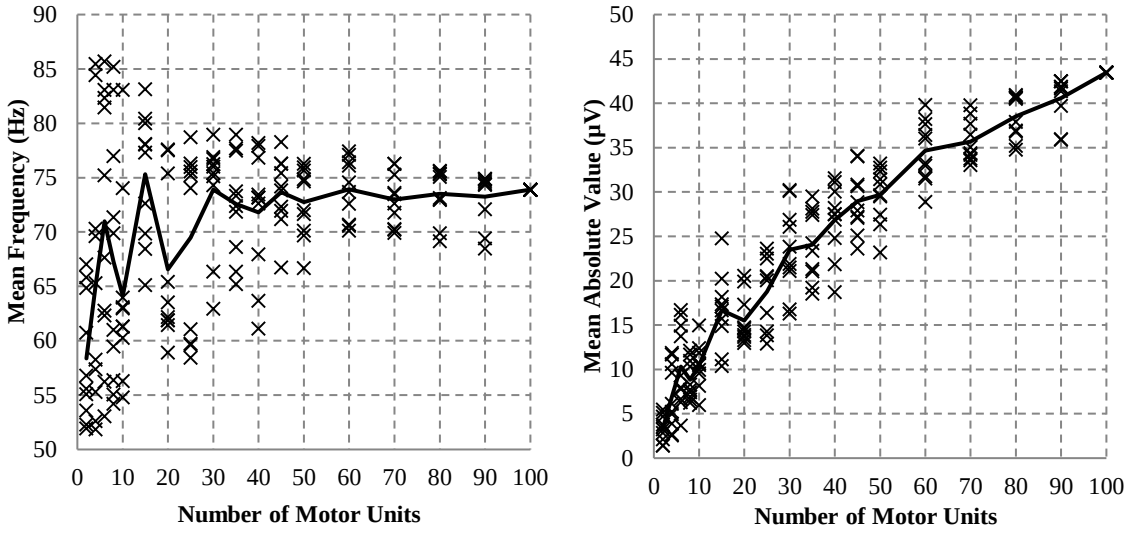

(a) (b)

Figure 2-8: Effect of motor unit recruitment on a) MF, b) MAV, with 10 combinations per NMU chosen from a pool of 100 motor units (included in the reference signal SEMG), investigated using simulated SEMG. Individual estimates are shown as crosses and the solid lines indicate average across 10 combinations. Results for reference signal shown at NMU=100.

For NMU>25, for MF, CoV was $\mu \pm \sigma = 3.16 \pm 0.23\%$. This is consistent with expected baseline variability in CoV values ($2.96 \pm 0.34\%$). For NMU<25, the variability in CoV is higher, indicating the influence of motor unit recruitment on MF variability for low NMU.

For NMU>50, for MAV, CoV was $\mu \pm \sigma = 4.75 \pm 0.18\%$. This is consistent with expected baseline variability in CoV values ($4.40 \pm 0.32\%$). For NMU<50, the variability in CoV is

higher, indicating the influence of motor unit recruitment on MAV variability for low NMU.

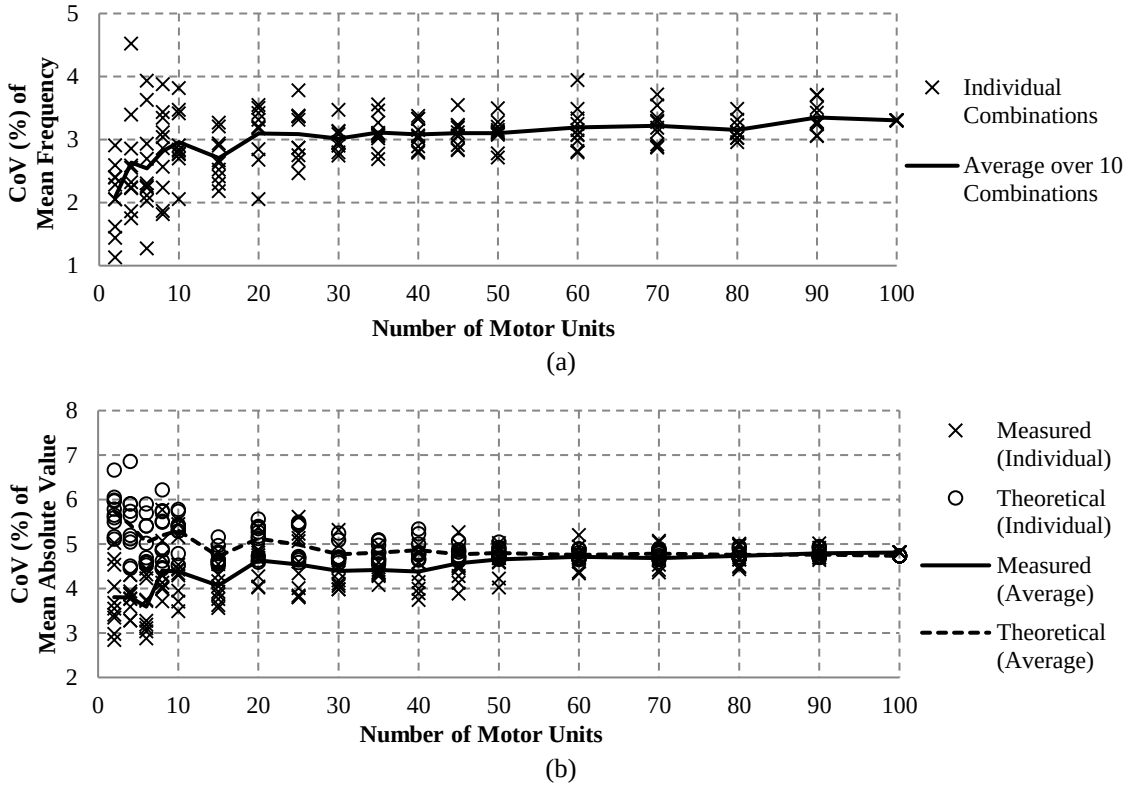

Figure 2-9: Effect of motor unit recruitment on the CoV of a) MF b) MAV estimates from simulated SEMG. At each NMU value, 10 combinations are shown along with their mean. Theoretical values of MAV estimates are shown in (b). Results for reference signal shown at NMU=100.

2.4 Discussion

Results depicted in Figure 2-2 confirm the expected effect of segment length on feature variability, for both MF and MAV. While variability decreases with increases to segment length for stationary signals like the one simulated to demonstrate this result, it is often not feasible to collect long records for processing during in vivo experimentation, or when using SEMG-based devices. In some cases, like myoelectric control, segment length must be kept very short, for example 160ms (Robertson, et al., 2018), to avoid the effects of delay. In other cases, like fatigue assessment, the segment length must be kept

sufficiently short (typically less than 10 sec, although this depends on the contraction and estimation approach used to assume stationarity within each segment (Farina & Merletti, 2000; Rogers & MacIsaac, 2010; Thongpanja, et al., 2013). While optimal segment length is application dependent, the results here show that it is prudent to choose as long a record length as possible when designing an SEMG experiment, or SEMG-based device. For applications that require segment lengths less than 1s, segment length will become a significant contributor to baseline variability.

Although longer segments produce more precise feature estimates, 1-second segments were chosen for analysis in this work since this has been shown to be an upper limit for maintaining stationarity (Inbar & Noujaim, 1984) for the types of contractions being analyzed here, and since 1-second segments are practical for many EMG studies. The simulation results depicted in Figure 2-3 and Figure 2-4 indicate that baseline variability measured by CoV can be expected to be around 3% for MF and 4.5% for MAV, at least for isometric/isotonic bicep contractions of strengths between 15-25% MVC (recall that the simulation data was matched to these conditions). Note that the theoretical CoV values for MAV are very similar to the baseline values from simulation.

The statistical comparison between simulated results and within-trial results indicated that the expected variability was observed for MF, but not for MAV: CoV values were higher in the within-trial records for MAV. Because the aim for the simulation was to get an accurate estimate of CoV, and the number of segments available was unlimited, 100 segments were included. In comparison, to avoid fatigue, only 15 segments were available in the within-trial records; thus, the simulation provided a more accurate estimate. However, given the sizable discrepancy in average CoV values (4.40±0.32%

from simulation vs. 12.00±4.84% from within-trial records), it is unlikely that better accuracy accounts for the difference observed. Indeed, when re-analyzed using only 15 segments in simulation, changes were minimal (4.22±0.8%). Thus, the increase in variability observed in MAV during the within-trial tests suggests that factors other than sampling error had an influence.

Results from the sensitivity analysis provide some guidance for attributing variability beyond the baseline to particular factors. Assuming the contributions from both sampling error and any additional variability are additive and uncorrelated, an estimate of the additional variability can be calculated. The total CoV measured from any *in vivo* record can be described as:

$$CoV_T^2 = CoV_\alpha^2 + CoV_\beta^2 \qquad \textbf{2-6}$$

where CoV_α is the expected variability due to sampling error and CoV_β is the variability introduced by other factors. Using this relationship and the estimate of CoV_α observed through simulation, the amount of additional variability can be determined. A CoV_T of 12.00% was observed in the MAV of within-trial records while a CoV_α of 4.40% was observed in MAV in simulation; thus, CoV_β in the MAV of within-trial records is $\sqrt{12.00^2 - 4.40^2}\% = 11.16\%$. This value represents an estimate of the expected variability in MAV due to random variability in factors like average fibre depth, CV, or NMU during a contraction that subjects are trying to hold static.

The amount of change in a particular factor required to yield the observed additional variability can be estimated using results from the sensitivity analysis. The analysis provided an estimate of the expected change in feature value per unit change in factor. Converting these values to *percent* change in feature per unit change in factor provides a

comparison between CoV_β and sensitivity if we interpret the sensitivity as the expected change in feature given a random variation in a particular factor with a standard deviation of 1. These percent sensitivity values are provided in Table 2-3. Ranges are provided to encapsulate percent sensitivity across factor values depicted in Figure 2-6 and Figure 2-7. The percent sensitivity $\%\Delta x_o$ for an absolute sensitivity value Δx_o at feature value x_o was calculated according to:

$$\%\Delta x_o = \frac{\Delta x_o}{x_o} \times 100\% \qquad \textbf{2-7}$$

Feature	Sensitivity to		
	Average Fibre Depth	Conduction Velocity	Number of Motor Units
MF	1.6-12%/mm	15-22%/m/s	0%/NMU*
MAV	13-28%/mm	39-60%/m/s	4%/NMU**

*For NMU>25; ** For NMU>50.

Table 2-3: Percent sensitivities for MF and MAV (calculated from the absolute sensitivity data).

Dividing CoV_β by percent sensitivity yields the standard deviation of the random variation in a factor required to yield the additional variability observed in a feature. If average fibre depth were to account for the 11.16% CoV_β in the MAV of within-trial records observed in this work, a random variation in depth would have to exist across segments, with a standard deviation of 0.40-0.86mm. Likewise, standard deviations required to account for the additional variability through the other factors would be 0.19-0.29m/s for CV and 2.8 for NMU. Given these values, the degree to which each factor would have to change in order to account for the additional variability observed is reasonable to expect in practice.

The observations made about MF help to narrow down the likely factors contributing to the additional variability in MAV. Since little additional variability was observed in the MF of within-trial records, it is unlikely that depth or CV had much contribution to the

additional variability in MAV, as these factors affect MF and MAV simultaneously. Conversely, NMU has little affect on MF, but MAV is sensitive to NMU. It is feasible therefore, to explain the observed additional variability of MAV in within-trial records by a recruitment pattern that adds and removes units of similar depths and CVs throughout the contraction.

The total variability in MAV for between-trial records was $CoV_{\mathrm{T}} = 14.83\%$. This was statistically higher than both baseline and within-trial tests, suggesting that a different pool of motor units may be recruited each time a contraction restarts. The total variability in MF for between-trial records was CoV_{T} of 4.08%. Unlike within-trial tests, increased variability in MF was also statistically significant in the between-trial tests. Thus, it is feasible that the pools of units recruited also had varying average depths, and/or CVs.

Additional variability in MAV for the between-trial records was estimated to be $CoV_{\beta} = 14.16\%$. The standard deviation of random variations in a factor required to account for this additional variability would be 0.51-1.09mm for average fibre depth, 0.24-0.36m/s for CV and 3.5 for NMU. Additional variability in MF for the between-trial records was estimated to be $CoV_{\beta} = 2.81\%$. The standard deviation of random variations in a factor required to account for this additional variability would be 0.23-1.76mm for average fibre depth, and 0.13-0.19m/s for CV. Again, the degree to which each factor would have to change in order to account for the additional variability observed is reasonable to expect in practice.

2.5 Conclusions

The aim of this work was to estimate the expected baseline variability in SEMG feature measurements using simulation, and then examine the possible sources of the additional variability observed during *in vivo* experiment under same session, within-trial and between-trial protocols. Based on the results of this work, for 1-second signal segments, a baseline variability of about 2.96% in MF and 4.40% in MAV can be expected when everything is held stationary. However, since both parameters were found to be sensitive to physiological factors average fibre depth, CV and NMU, it is unlikely that observed variability will be as low as the baseline in measurements, except under the strictest conditions. It is possible to meet these conditions for MF as demonstrated by the within-trial test during which MF variability did not increase beyond the expected baseline. However, the same cannot be said for MAV, which yielded an increase in variability, even during the within-trial test (12.00%). For the between-trial test, an increase in variability was observed for both features (4.08% and 14.83% respectively). This work shows that factors other than sampling error have influence on SEMG parameters, even during short, static, non-fatiguing contractions, and that restarting a contraction increases the influence. The effects are likely due to recruitment patterns switching between motor units during contraction. Since there were no significant differences noted between the contractions levels, this conclusion holds for contractions between 15-25%.

REFERENCES

Arnall, F., Koumantakis, G., Oldham, J. & Cooper, R. (2002) 'Between-days reliability of electromyographic measures of paraspinal muscle fatigue at 40, 50 and 60% levels of maximal voluntary contractile force'. *Journal of Clinical Rehabilitation,* 16(7), pp. 761-771.

Carius, D., Kugler, P., Kuhwald, H. & Wollny, R. (2015) 'Absolute and relative intrasession reliability of surface EMG variables for voluntary precise forearm movements'. *Journal of Electromyography and Kinesiology,* 25(6), pp. 860-869.

Clancy, E. (1999) 'Probability Density of the Surface Electromyogram and Its Relation to Amplitude Detectors'. *IEEE Transactions on Biomedical Engineering,* 46(6), pp. 730-739.

Farina, D., Holobar, A., Merletti, R. & Enoka, R.M. (2010) 'Decoding the neural drive to muscles from the surface electromyogram'. *Clinical Neurophysiology,* 121(10), pp. 1616-1623.

Farina, D. & Merletti, R. (2000) 'Comparison of algorithms for estimation of EMG variables during voluntary isometric contractions'. *Journal of Electromyography and Kinesiology,* 10(5), pp. 337-349.

Farina, D., Merletti, R. & Enoka, R.M. (2004a) 'The extraction of neural strategies from the surface EMG'. *Journal of Applied Physiology,* 96(4), pp. 1486-1495.

Farina, D., Merletti, R. & Stegeman, D. (2004b) 'Biophysics of the generation of EMG signals'. In: R. Merletti & P. Parker, eds. *Electromyography: physiology, engineering, and non-invasive applications.* Hoboken: John Wiley & Sons, Inc., pp. 81-105.

González-Cueto, J. & Parker, P. (2002) 'Deconvolution Estimation of Motor Unit Conduction Velocity Distribution'. *IEEE Transactions On Biomedical Engineering,* September, 49(9), pp. 955-961.

Huckabee, M., Low, I.S. & McAuliffe, M.J. (2012) 'Variability in Clinical Surface Electromyography Recording of Submental Muscle Activity in Swallowing of Healthy Participants'. *Asia Pacific Journal of Speech, Language and Hearing,* 15(3), pp. 175-186.

Inbar, G.F. & Noujaim, A.E. (1984) 'On Surface EMG Spectral Characterization and Its Application to Diagnostic Classification'. *IEEE Transactions on Biomedical Engineering,* 31(9), pp. 597-604.

Lee, J., Adam, A. & De Luca, C.J. (2008) 'A simulation study for a surface EMG sensor that detects distinguishable motor unit action potentials'. *Journal of Neuroscience Methods,* 168(1), pp. 54-63.

Lovely, D.F. (1993) 'Low noise electrode amplifier for use in evoked potential studies'. *Proceedings of 19th Canadian Medical & Biological Engineering Society Conference,* pp. 236-237.

MacIsaac, D., Rogers, D. & Bhandarkar, A. (2006) 'Simulating Myoelectric Signals with a Finite-Length Model of Muscle'. *Proceedings of the 29th Conference of the Canadian Medical and Biological Engineering Society*. Vancouver, Canada.

MacIsaac, D., Tallam Puranam Raghu, S. & Shi, Y. (2018) 'MyoSim 2.0: Enhancing And Validating an EMG Simulation Tool'. *Proceedings of the 41st Conference of the Canadian Medical and Biological Engineering Society*. Charlottetown, PEI, Canada.

Mathur, S., Eng, J. & MacIntyre, D. (2005) 'Reliability of surface EMG during sustained contractions of the quadriceps'. *Journal of Electromyography and Kinesiology,* 15(1), pp. 102-110.

McGraw, K. & Wong, S.P. (1996) 'Forming Inferences About Some Intraclass Correlation Coefficients'. *Psychological Methods,* 1(1), pp. 30-46.

Merletti, R., Farina, D. & Gazzoni, M. (2003) 'The linear electrode array: a useful tool with many applications'. *Journal of Electromyography and Kinesiology,* February, 13(1), pp. 37-47.

Merletti, R., Farina, D. & Granata, A. (1999) 'Non-invasive assessment of motor unit properties with linear electrode arrays'. *Electroencephalography and Clinical Neurophysiology,* 50(supplementary), pp. 293-300.

Merletti, R., Rainoldi, A. & Farina, D. (2001) 'Surface Electromyography for Noninvasive Characterization of Muscle'. *Exercise & Sport Sciences Reviews,* January, 29(1), pp. 20-25.

Parker, P., Stuller, J. & Scott, R. (1977) 'Signal processing for the multistate myoelectric channel'. *Proceedings of the IEEE,* 65(5), pp. 662-674.

Plonsey, R. (1974) 'The active fiber in a volume conductor'. *IEEE Transactions on Biomedical Engineering,* Sept., 21(5), pp. 371-381.

Rainoldi, A., Galardi, G., Maderna, L., Comi, G., Lo Conte, L. & Merletti, R. (1999) 'Repeatability of surface EMG variables during voluntary isometric contractions of the biceps brachii muscle'. *Journal of Electromyography and Kinesiology,* 9(2), pp. 105-119.

Rainoldi, A., Melchiorri, G. & Caruso, I. (2004) 'A method for positioning electrodes during surface EMG recordings in lower limb muscles'. *Journal of Neuroscience Methods,* 15 March, 134(1), pp. 37-43.

Rainoldi, A., Nazzaro, M., Merletti, R., Farina, D., Caruso, I. & Gaudenti, S. (2000) 'Geometrical factors in surface EMG of the vastus medialis and lateralis muscles'. *Journal of Electromyography and Kinesiology,* Volume 10, p. 327–336.

Robertson, J.W., Englehart, K.B. & Scheme, E.J. (2018) 'Rejection of Systemic and Operator Errors in a Real-Time Myoelectric Control Task'. *Proceedings of 40th Annual International Conference of the IEEE Engineering in Medicine and Biology Society (EMBC)*. Honolulu, HI.

Rogers, D.R. & MacIsaac, D.T. (2010) ‘Training a multivariable myoelectric mapping function to estimate fatigue’. *Journal of Electromyography and Kinesiology,* 20(5), pp. 953-960.

Scheme, E. & Englehart, K. (2011) ‘Electromyogram pattern recognition for control of powered upper-limb prostheses: State of the art and challenges for clinical use’. *Journal of Rehabilitation Research and Development,* 48(6), pp. 643-59.

Shenoy, S. (2010) ‘EMG in sports rehabilitation’. *British Journal of Sports Medicine,* 44(Suppl 1), pp. i10-i10.

Shrout, P. & Fleiss, J. (1979) ‘Intraclass Correlations: Uses in Assessing Rater Reliability’. *Psychological Bulletin,* 86(2), pp. 420-428.

Suzuki, H., Conwit, R., Stashuk, D., Santarsiero, L. & Metter, E.J. (2002) ‘Relationships between surface-detected EMG signals and motor unit activation’. *Medicine & Science in Sports & Exercise,* 34(9), pp. 1509-1517.

Tallam Puranam Raghu, S. (2017) ‘Baseline Noise and Model Parameters in Surface Electromyography’, MScE Thesis, Department of Electrical and Computer Engineering, University of New Brunswick, Fredericton, Canada.

Thongpanja, S., Phinyomark, A., Phukpattaranont, P. & Limsakul, C. (2013) ‘Mean and Median Frequency of EMG Signal to Determine Muscle Force based on Time-Dependent Power Spectrum’. *ELEKTRONIKA IR ELEKTROTECHNIKA,* 19(3), pp. 51-56.

Wheeler, K., Kumar, D. & Shimada, H. (2010) ‘An Accurate Biceps Muscle Model with sEMG and Muscle Force Outputs’. *Journal of Medical and Biological Engineering,* 30(6), pp. 393-398.

Yao, W., Fuglevand, R.J. & Enoka, R.M. (2000) ‘Motor-Unit Synchronization Increases EMG Amplitude and Decreases Force Steadiness of Simulated Contractions’. *Journal of Neurophysiology,* 83(1), pp. 441-452.

CHAPTER 3 A SIGNAL QUALITY INDEX FOR ELECTRODE LOCATION USING SINGLE-CHANNEL SURFACE EMG FEATURES

3.1 Introduction

The importance of proper electrode placement during surface electromyography (SEMG) has been addressed by many studies. Specifically, the importance of placing electrodes carefully to avoid innervation zones (IZ) (Rainoldi, et al., 2000; Rainoldi, et al., 2004; Farina, et al., 2001) and tendon regions (Rainoldi, et al., 2000; Masuda, et al., 1985; Merletti, et al., 2001a; Roy, et al., 1986) has been emphasized. Placing electrodes in these regions can cause poor signal quality for two major reasons. First, signals containing incomplete and non-propagating action potentials will be collected (Farina, et al., 2004). Second, action potentials passing under electrodes placed in a bipolar configuration within the IZ will be detected with opposite phases, causing cancellation and distorted action potentials to be collected (Merletti, et al., 1999). Placing electrodes over IZs or tendon regions can significantly alter estimated feature values from SEMG signals (Rainoldi, et al., 2004; Masuda, et al., 1985; Roy, et al., 1986; Merletti, et al., 2001b), making proper electrode placement an important consideration for applications which rely on such features, including SEMG-based assistive devices and diagnostic tools.

The multi-channel linear electrode array has been a powerful tool for studying the effects of IZ and tendon regions, and can be used to identify them during data collection. As shown in Figure 3-1, the location of an IZ can be identified by noting channels along the array where phase reversal occurs and/or with low signal amplitude (Masuda, et al., 1985; Merletti, et al., 2003). IZ location can also be spotted from conduction velocity (CV) estimates based on cross-correlation analysis since their signs change for channels

located on different sides of the IZ and their values become invalid for a channel over IZ (Merletti, et al., 2003). The value of CV estimates may also become invalid for channels affected by tendons, due to the detection of non-propagating action potentials and the termination effect of propagating action potentials. A decrease in amplitude is also generally observed as channels in the array approach tendon regions (Rainoldi, et al., 2004) and increases in mean frequency values have been noted as channels approach IZs and tendon regions (Rainoldi, et al., 2004; Merletti, et al., 2003).

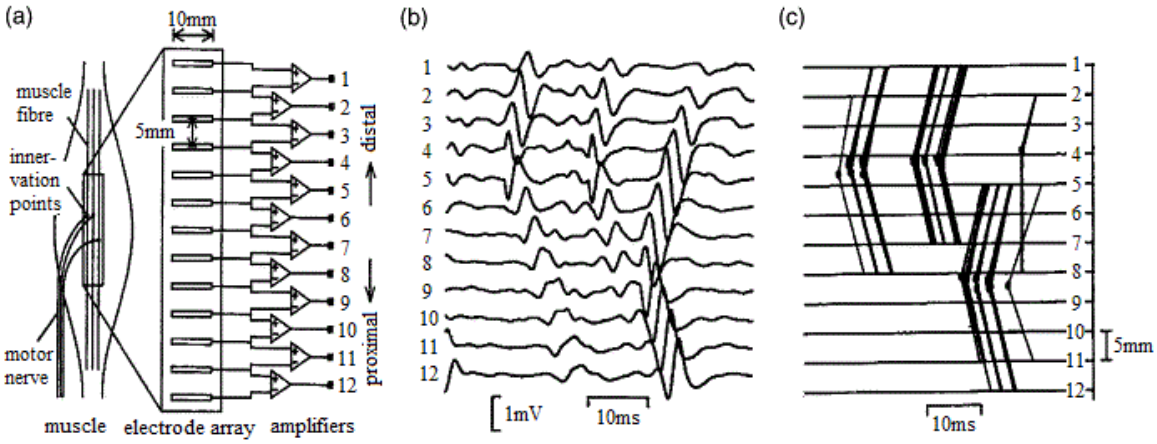

Figure 3-1: a) A schematic representation of the detection modality with linear electrode arrays (single differential recording). b) A typical signal recorded from the biceps brachii muscle (interelectrode distance 5 mm). c) Location of the IZs (dots where lines start) for the recording shown in (b). (Masuda, et al., 1985)

Compared to single-channel SEMG, collecting and analyzing multi-channel SEMG data requires longer set-up times, more extensive equipment, and expertise of the user. When using is practical, an approach proposed by Kendell et al. (2012) can be applied to select the best channel for analysis. However, due to the added complexity associated with multi-channel SEMG, single-channel SEMG is still commonly used (Gazzoni, 2016; Merlo & Campanini, 2016). Example applications include biofeedback (Sturma, et al., 2018), sport science (Hug & Tucker, 2017) and diagnosis of neuromuscular conditions (Naik, et al., 2016). Since some applications SEMG require only a single channel of data, it would be convenient to have a way to determine acceptable electrode locations by

analyzing single-channel data. The purpose of this work was to examine features extracted from multiple channels of SEMG data to determine if any of the features are suitable as a signal quality index sensitive to poor electrode placement, based on single-channel data.

The ideal feature for a signal quality index would be one that shows a significant difference between signals obtained from channels affected by IZs/tendons and those unaffected, in a consistent way across subjects. In this work, numerous features extracted from SEMG recordings collected with an electrode array were tested to determine if one or more have a definitive gap in value between channels that are ill-affected and those that are not. The aim was to distinguish between affected and unaffected channels with an index threshold consistent across subjects, so that the index could be used to automatically classify signals of low quality due to poor electrode placement, in a systematic way.

In their work, Merletti et al. (2003) noted that proximity to the IZ and tendon regions cause incomplete and non-propagating action potentials to have influence on the measured SEMG. These effects can influence the shape of the waveform and both shift and skew its spectrum. Based on this, a broad range of features were tested for sensitivity and consistency across subjects. Features reported here include: mean frequency, normalized bandwidth, kurtosis of the bandlimited power spectrum, band power ratio, and absolute area of a normalized action potential. It is worth noting that preliminary studies using features established in other work as generally able to characterize SEMG (Fraser, et al., 2014) were also initially considered but yielded less consistent results than those reported here. These included four-term autoregressive model coefficients, 10th bin

of SEMG amplitude histogram, mean absolute value, 10-bin averaged power spectral density, number of slope sign changes, Willison amplitude, waveform length, and number of zero crossings.

3.2 Methods

In this work, SEMG data were collected with a linear electrode array from the bicep brachii of ten subjects during maximum voluntary contractions (MVC). Features were extracted from signals measured at each channel to observe how they varied across channels, and in particular to compare values from channels close to and far from IZs and tendon regions. To establish a standard upon which to judge each feature as a signal quality index, channels near to the IZs or tendon regions had to be identified, and since individuals have differing physiologies, this had to be done on a subject-by-subject basis. To do so, three experts examined data from each channel and established consensus for each subject in identifying the channels as either sufficiently close to IZs/tendon regions to affect the signal, or sufficiently far to have negligible effect. Those affecting the signal were assumed to yield poor quality signals and were identified as low quality (LQ) channels. Those unaffected were assumed to yield good quality signals and were identified as high quality (HQ) channels. Experts considered electrode location (the ends of the array, or near the belly of the muscle) in their evaluation but also considered 3 corroborating factors, all based on cross-correlation between signals measured from adjacent channels: magnitude and sign of conduction velocity, symmetry in the cross-correlation function, and cross power, estimated by the peak of the cross-correlation.

3.2-1 Data Collection

Data collection was performed with a linear electrode array which included eight pre-gelled Ag/AgCl electrodes (circular conductor with diameter 11mm) placed along the subject's biceps brachii. A reference electrode was placed on the back of each subject's neck. The electrodes and amplifiers were configured similar to what is shown in Figure 3-1a, but with an interelectrode distance of 20mm (centre to centre) and only seven channels as shown in Figure 3-2. Adjacent channels shared one electrode and channel 1 to 7 spread from the distal to proximal end of the upper arm, with channel 1 located closest to the elbow. The electrodes were connected to a Grass® F-15EB/B1 electrode board, which routed the signals to Grass® 15A54 quad amplifiers. The amplifiers have built-in configurable high-pass and low-pass filters, whose cut-off frequencies were set to 3Hz for the high-pass and 1000Hz for the low-pass during the tests. The gain of the amplifiers ranged from 500 to 2000 so that the signal amplitude was maximized for each subject without saturating the amplifiers or data acquisition board (DAQ). The amplified signals were fed into a National Instruments® USB-6216 DAQ, where they were sampled at 3000Hz and quantized at 16-bit. Finally, the digital signals were sent to a computer via USB connection for offline processing.

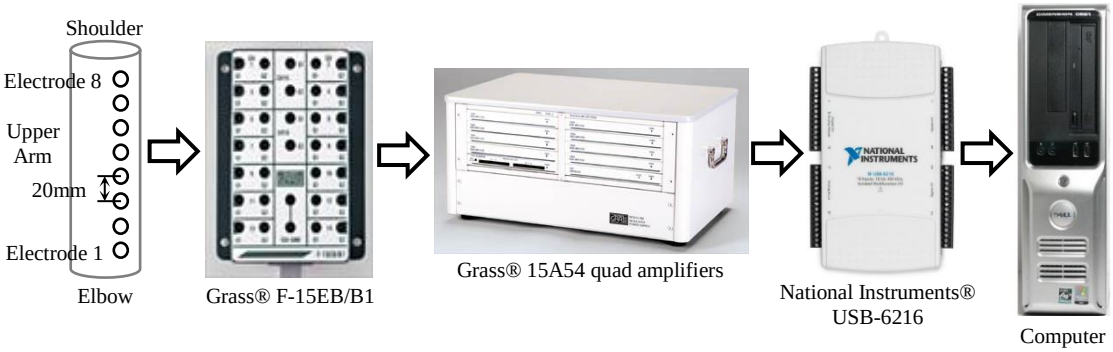

Figure 3-2: Diagram of SEMG data collection equipment setup.

SEMG data was collected from the bicep brachii muscles of ten subjects (seven males and three females, age 21.0±2.0). Before each test, skin preparation was done by rubbing with Nuprep® abrasive gel followed by cleaning with isopropyl alcohol. The electrode array was then attached to the upper arm along the subject's bicep brachii. Channel cables were affixed to surrounding skin with sport tape to minimize wire movement and potential false contact. After proper electrodes affixation, the impedances between each pair of the electrodes (i.e. each channel) were measured to ensure good contact. Skin preparation was repeated when the measurement was higher than 10kΩ.

Data was collected from each subject during rest and MVC. For rest data, the subjects were asked to relax the upper arm so that no action potential was observed during a 10-second recording used to measure background noise level. The choice to use MVC during activation was made so that most motor units and the full muscle cross-section was represented in the measurement. For MVC recordings, subjects were asked to push upward against the bottom of an unmovable platform with the elbow flexed at about 90°. A total of three MVC trials were performed with just over 3 seconds of contraction for each, with 60 seconds of rest between trials. The collected data was visually inspected in both time and frequency domains to ensure that they were free of excessive background noise. Trials with noticeable noise were discarded and repeated. Then a 3-second record was extracted from the middle of each trial. The trial record with the most consistent amplitude (determined the per-0.33s mean absolute values) for each subject was selected for analysis.

3.2-2 Data Processing

For each subject, five features were calculated from the 3-second segments measured during MVC at each channel. Four of the features were based on a power spectral estimate. When the estimate was calculated with a Welch's spectral estimator, Hamming windows of duration $T_{\mathrm{w}} = 0.67\mathrm{s}$ were used with a 50% overlap. When a Burg's estimator was used, the order of the autoregressive model was set to 12. Further details regarding each feature calculation are delineated below:

1. Mean frequency (MF) is a weighted average frequency of the power spectral density (PSD). First, the PSD $\Phi_{xx}(f)$ was calculated using Welch's estimator. Then MF was calculated according to

$$MF = \frac{\sum_{m=1}^{M} f_m \Phi_{xx}(f_m)}{\sum_{m=1}^{M} \Phi_{xx}(f_m)} \qquad \textbf{3-1}$$

where M is the length of the PSD, f_m is the frequency of the m^{th} component in the PSD and $\Phi_{xx}(f_m)$ is the magnitude of the PSD at frequency f_m.

2. Normalized Bandwidth (NBW) was calculated by first obtaining a PSD estimate using Burg's autoregressive estimator. This estimator was chosen because it yields a PSD free of fluctuation with monotonic ascending and descending intervals. This simplified the searching process for the parameters used to calculate NBW. The bandwidth was considered to be the difference between upper corner frequency $f_{\mathrm{c,hi}}$ and lower corner frequency $f_{\mathrm{c.lo}}$ where PSD amplitudes were -3dB relative to the maximum amplitude. Then the bandwidth was normalized by f_{max}, the frequency which corresponded to the maximum amplitude of the PSD:

$$NBW = \frac{f_{\mathrm{c,hi}} - f_{\mathrm{c,lo}}}{f_{\mathrm{max}}} \qquad \textbf{3-2}$$

3. Kurtosis (KUR) is a measure which can reflect the flatness of a distribution, and how often a distribution tends to have outliers (Westfall, 2014). In this work, the PSD of each channel, bandlimited to twice the corresponding mean frequency estimate, was treated as a distribution whose Kurtosis was calculated. First the PSD was estimated using Welch's estimator, and then normalized by the total power according to:

$$\widetilde{\Phi}_{xx}(f_m) = \frac{\Phi_{xx}(f_m)}{\sum_{m=1}^{M} \Phi_{xx}(f_m)} \quad \textbf{3-3}$$

where M is the length of the PSD, f_m is the frequency of the m^{th} component in the PSD and $\Phi_{xx}(f_m)$ is the magnitude of PSD at frequency f_m. Then the bandlimited PSD $\widehat{\Phi}_{xx}(f_m)$ was obtained through truncating $\Phi_{xx}(f_m)$ to twice the corresponding MF. Finally, KUR was calculated using the Pearson moment (Fiori & Zenga, 2009) since it is commonly-used and easy to implement. This moment defines Kurtosis as:

$$KUR = \frac{\mathrm{E}[(x-\mu)^4]}{\sigma^4} \quad \textbf{3-4}$$

where x is a random variable with μ as its mean, and σ^2 as its variance. Accordingly, for a distribution given by $\widehat{\Phi}_{xx}$, its mean μ is the mean frequency given by Equation 3-1 and its variance is given by:

$$\sigma^2 = \mathrm{E}[(x-\mu)^2] = \sum_{m=1}^{M'} (f_m - \mu)^2 \widehat{\Phi}_{xx}(f_m) \quad \textbf{3-5}$$

The numerator of Equation 3-4 is thus

$$\mathrm{E}[(x-\mu)^4] = \sum_{m=1}^{M'} (f_m - \mu)^4 \widehat{\Phi}_{xx}(f_m) \quad \textbf{3-6}$$

where M' is the length of the bandlimited PSD.

4. The band power ratio (BPR) is a ratio of power above and below a threshold frequency f_{TH}. For this work, the PSD was calculated using Welch's estimator and the threshold was set to $f_{\mathrm{TH}} = 110\mathrm{Hz}$. This threshold was chosen based on observations made by Beck et al. (2009) while examining the influence of electrode placement over IZs on low vs. high bands of the SEMG frequency spectrum.

5. The absolute area of a normalized action potential (AANAP) is the area under the absolute value of an averaged motor unit action potential (AMUP) waveform obtained from normalized SEMG recordings using a spike-triggered ensemble averaging scheme proposed by Lang et al. (1971) and slightly modified by Viitasalo and Komi (1975). To extract an AMUP, spike peaks were first located in the SEMG segment that was normalized by its maximum value. The normalization of SEMG recordings by their respective maximum values makes AMUP waveforms comparable across channels. Spike peaks were found by locating the local maximums for all sections of the signal that were above a threshold in normalized absolute amplitude set to $A_{th} = 0.5$, and at least 10ms (30 samples) away from any other peaks. For the M spikes identified, individual waveforms were extracted taking 20.3ms centered around each peak (30 samples on each side of the peak sample). An ensemble average was taken across the M individual waveforms resulting in an AMUP waveform of 20.3ms for each channel. Then the AANAP values were obtained as the area under absolute values of these waveforms.

3.2-3 Data Analysis

With features calculated for each channel, and all channels near the IZs/tendon regions identified by experts, an analysis was conducted to compare performance of the features

as a signal quality index. Two performance metrics were used, both based on measuring a feature's ability to distinguish between LQ and HQ channels.

First, a clustering analysis technique was used to quantify the separability of feature values from LQ and HQ channels (labeled according to expert evaluation). This technique, known as a silhouette analysis, is widely used in data mining applications to determine the number of clusters in a data set when applying the K-means clustering algorithm (Kaufman & Rousseeuw, 1990). First, a silhouette value for each feature value i in the HQ cluster was calculated according to

$$s(i) = \frac{LQ(i) - HQ(i)}{\max\{LQ(i), HQ(i)\}} \quad \text{3-7}$$

where $HQ(i)$ is the average distance of i to all other samples in HQ and $LQ(i)$ is the average distance of i to all the samples in LQ. Since feature values are 1-dimensional, distance is simply calculated as the absolute difference between two values. Then the silhouette values for each element were averaged to obtain the measure of separability, S, for the feature. This metric varies between -1 to 1 and values closer to 1 indicate samples in HQ are much closer to their own cluster than they are to values in LQ. This measure of separability was calculated for each feature across all subjects.

Next, a threshold was set for each feature that aimed to separate HQ channels from LQ channels. Channels that yielded feature values on one side of the threshold were classified as HQ channels according to that feature, while channels that yielded feature values on the other side were classified as LQ channels. The threshold was set to maximize overall classification accuracy using the results of expert evaluation as true classes (i.e. labels). Accuracy was quantified as a percentage of channels correctly

categorized by the threshold as either HQ or LQ, assuming the expert classifications to be 100% accurate. For comparison purposes, accuracies were also broken down in terms of LQ as affected by IZs vs tendon regions. From an application perspective, it is more consequential to keep data from LQ channels than it is to discard data from HQ channels, so a measure of how many of the channels classified by each feature as HQ were wrongly classified is also useful; thus the misclassification rate of HQ channels by feature is also reported, calculated as:

$$\varepsilon_{HQ} = \frac{n_{HQ,wrong}}{n_{HQ,total}} \qquad \textbf{3-8}$$

where $n_{HQ,total}$ is the total number of channels classified as HQ with the set threshold and $n_{HQ,wrong}$ is the number of channels among them that were wrongly classified as HQ.

3.3 Results

3.3-1 Expert Evaluation of Channel Quality

Figure 3-3 depicts the set of cross-correlation plots for adjacent channels of Subject 4. Conduction velocity (CV), cross-power (peak), and individual channel RMS powers are all indicated in the plot. Threshold values are also indicated which represent 15% of the mean of the RMS powers from the individual channels. Expert evaluators used these parameters collectively as a guide in classifying LQ and HQ channels. In classifying HQ channels, experts looked for reasonable CV values (ranging from 3-7 m/s), symmetry in the cross-correlation, a cross-power greater than the mean power threshold, and also took into consideration CV sign changes, and locations of the channel. In the example depicted, channel 4 was identified as an IZ-affected LQ channel and channel 7 was identified as a tendon-affected LQ channel. While the locations and values varied from

subject-to-subject, the trends delineated in Figure 3-3 are representative across the data set.

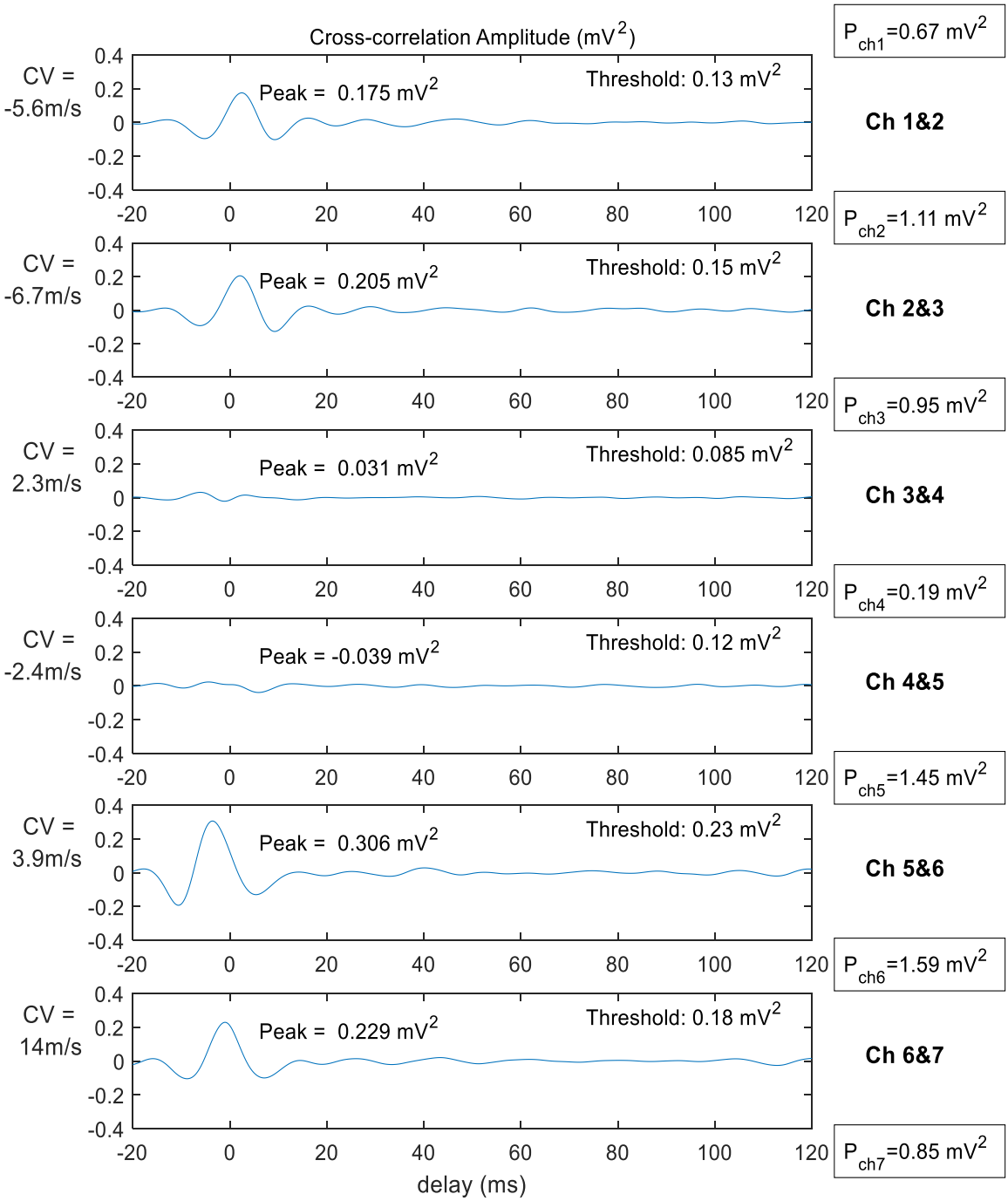

Figure 3-3: Cross-correlation plots for channels from Subject 4 that were used in expert evaluation. The CV estimates based on cross-correlation are shown on the left. The peak value of each cross-correlation plot (cross power) is shown and compared to a threshold, which is calculated as 15% the mean between the individual powers (shown on the right in boxes) of the two channels included in the cross-correlation.

Table 3-1 delineates the results of channel quality evaluation conducted by the three experts, greyscale-coded with lighter grey indicating channels affected by IZs and darker grey indicating channels affected by tendons. Of the 70 channels analyzed, 45 were classified as HQ channels while 13 were considered LQ channels affected by IZs and the remaining 12 were considered LQ channels affected by tendons.

Subject	Channel 1	Channel 2	Channel 3	Channel 4	Channel 5	Channel 6	Channel 7
1	Tendon	HQ	HQ	IZ	HQ	HQ	HQ
2	Tendon	HQ	HQ	IZ	HQ	HQ	Tendon
3	Tendon	HQ	HQ	IZ	IZ	HQ	HQ
4	HQ	HQ	HQ	IZ	HQ	HQ	Tendon
5	Tendon	HQ	HQ	IZ	IZ	HQ	HQ
6	Tendon	Tendon	HQ	HQ	HQ	IZ	HQ
7	HQ	HQ	HQ	IZ	HQ	HQ	HQ
8	Tendon	HQ	HQ	HQ	IZ	HQ	HQ
9	Tendon	HQ	HQ	HQ	IZ	HQ	HQ
10	Tendon	HQ	HQ	IZ	IZ	HQ	Tendon

Table 3-1: Channel quality expert evaluation results, with channels affected by IZ marked in lighter grey, tendon regions in darker grey and those unaffected by either (HQ channels) in white.

3.3-2 Performance of SEMG Features

Examples of power spectral estimates and AMUPs taken from an LQ channel (Subject 4, channel 4), and an HQ channel (Subject 4, channel 5) are shown in Figure 3-4 and Figure 3-5. Differences between HQ and LQ channels as shown in the figures are representative of the dataset in general.

In the example shown in Figure 3-4, corner frequencies and mean frequency are indicated on the PSD obtained using Burg's method. The PSD obtained from the HQ channel demonstrates lower MF and bandwidth, and higher Kurtosis compared to the LQ channel. It also demonstrates a difference in area on each side of f_{TH} which leads to lower BPR values for HQ channels. In the example shown in Figure 3-5, the AMUP obtained from the HQ channel (solid line) has a wider centre lobe and higher amplitude over the last 20 samples compared to the LQ channel (dashed line). In some cases an HQ channel may

also demonstrate higher amplitude in the first 20 samples. These observations are captured by the area under the waveforms and thus result in higher AANAP values for HQ channels compared to LQ channels.

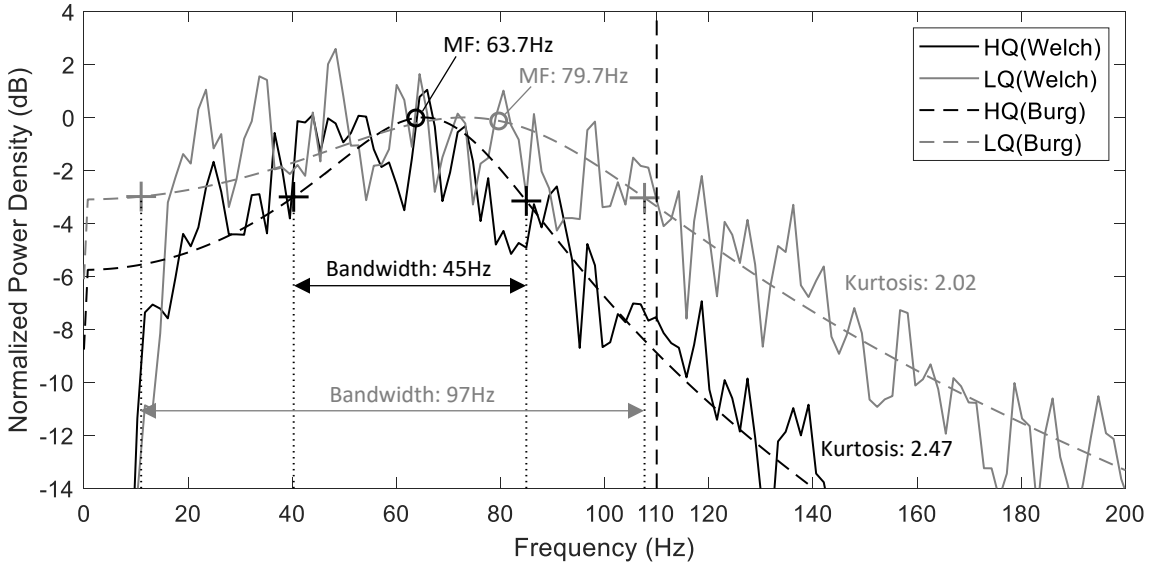

Figure 3-4: PSD estimates for channel 5 (HQ) and 4 (LQ) of Subject 4 using Welch's method with 0.67s Hamming windows and 50% overlap and Burg's method with a 12-order autoregressive model, scaled by the maximum amplitude in the Burg's PSD of each channel. The values of corner frequencies (-3dB), bandwidths, mean frequencies and 110Hz (f_{TH} of BPR) are indicated.

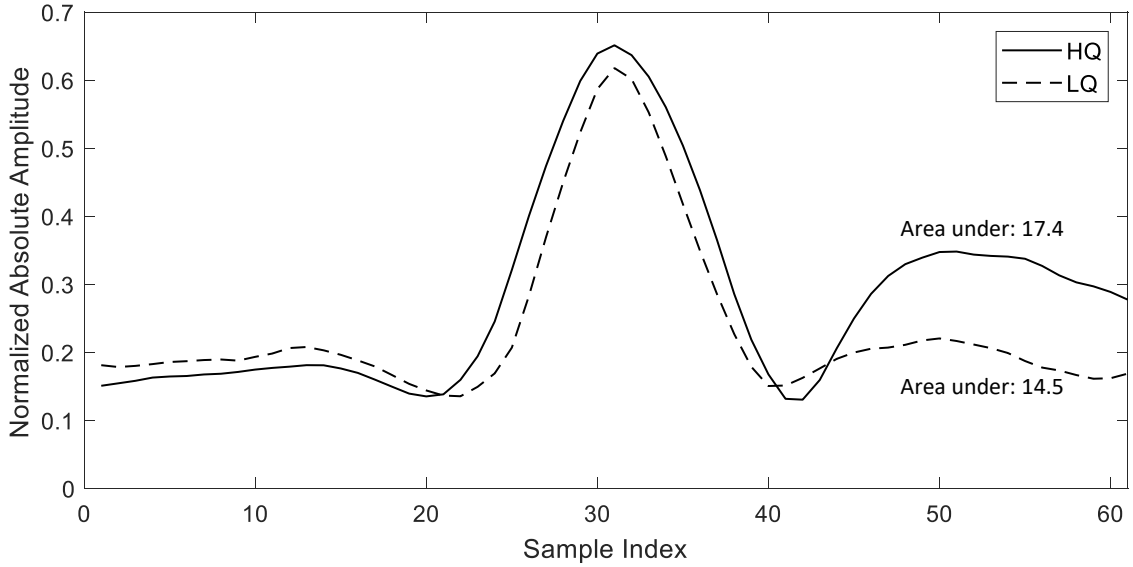

Figure 3-5: Absolute AMUP waveforms for channel 5 (HQ) and 4 (LQ) of Subject 4. The AANAP values were obtained as the area under these waveforms.

Table 3-2 to Table 3-6 delineate features values across all subjects and channels. For readability, channels which were classified as HQ by expert evaluation are highlighted in

yellow, and the channels which were classified as HQ based on feature value are bolded. For visual clarity, feature values are also plotted in Figure 3-6 to Figure 3-10. Accuracy and separability metrics are summarized in Table 3-7 and Table 3-8 respectively.

Table 3-2 delineates MF values across all subjects and channels. A threshold of 70Hz yielded the best overall classification accuracy at 75.7%. With the threshold set, MF correctly classified 33 of the 45 (73.3%) HQ channels (<70Hz) but 5 out of the 38 (13.2%) classified HQ channels were misclassified (4 of which were channels affected by tendons). Correspondingly, 12 out of 13 (92.3%) LQ channels affected by IZs and 8 out of 12 (66.7%) LQ channels affected by tendons were correctly classified.

Subject	Channel 1	Channel 2	Channel 3	Channel 4	Channel 5	Channel 6	Channel 7
1	91.1	70.1	**59.1**	77.0	77.7	**58.0**	**59.2**
2	75.6	85.0	71.0	75.2	76.7	**67.9**	82.2
3	**55.2**	**49.1**	**50.3**	70.1	**57.8**	**45.5**	**55.1**
4	81.1	**64.7**	**68.5**	79.7	**63.7**	**60.9**	71.6
5	73.2	78.6	**58.1**	83.8	81.1	**56.8**	**62.9**
6	**65.8**	**63.5**	**66.7**	**62.5**	**68.8**	81.3	**60.1**
7	**64.4**	**56.1**	**68.0**	86.9	**62.6**	**62.1**	**60.7**
8	**55.1**	**66.8**	**54.6**	**67.5**	77.4	**58.2**	**56.9**
9	78.5	82.4	**62.8**	81.6	112.4	**67.5**	**62.6**
10	84.4	83.3	94.4	96.6	106.5	105.3	79.7

Table 3-2: MF estimates from all subjects and all channels with HQ channels according to expert evaluation marked in grey and HQ channels according to the feature values and the set threshold (<70Hz) bolded.

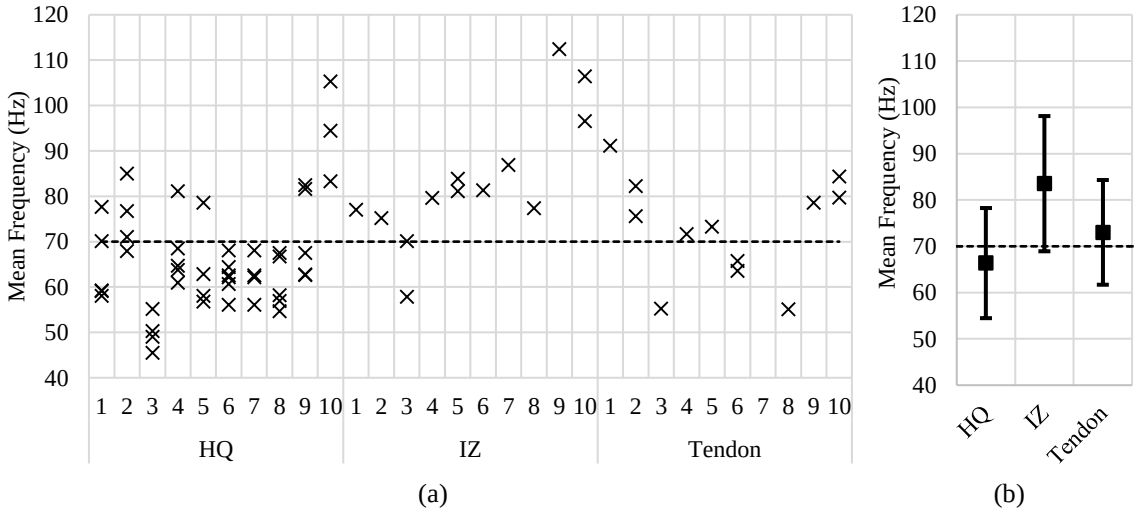

Figure 3-6: a) Scatter plot b) mean and standard deviation of MF estimates from all subjects grouped by reference channel location.

Table 3-3 delineates NBW values across all subjects and channels. A threshold of 0.9 yielded the best overall classification accuracy at 72.9%. With the threshold set, NBW correctly classified 38 of the 45 (84.4%) HQ channels (<0.9) but 12 out of the 50 (24%) classified HQ channels were misclassified (8 of which were channels affected by tendons). Correspondingly, 9 out of 13 (69.2%) LQ channels affected by IZs and 4 out of 12 (33.3%) LQ channels affected by tendons were correctly classified.

Subject	Channel 1	Channel 2	Channel 3	Channel 4	Channel 5	Channel 6	Channel 7
1	1.010	1.423	1.012	1.716	**0.850**	**0.702**	**0.893**
2	**0.782**	**0.673**	**0.510**	1.126	**0.557**	**0.637**	**0.830**
3	**0.662**	**0.522**	**0.437**	1.449	1.471	**0.719**	1.043
4	**0.663**	**0.539**	**0.733**	1.320	**0.685**	**0.690**	**0.899**
5	1.023	**0.820**	**0.631**	1.265	**0.713**	**0.568**	**0.783**
6	**0.516**	**0.352**	**0.371**	**0.344**	**0.489**	1.074	**0.393**
7	**0.548**	**0.295**	**0.573**	0.917	**0.267**	**0.543**	**0.550**
8	1.090	**0.670**	**0.617**	0.906	1.041	**0.398**	**0.833**
9	0.909	**0.867**	**0.886**	0.973	**0.716**	**0.581**	1.000
10	**0.587**	**0.453**	**0.664**	**0.541**	**0.757**	0.920	**0.636**

Table 3-3: NBW estimates from all subjects and all channels with HQ channels according to expert evaluation marked in grey and HQ channels according to the feature values and the set threshold (<0.9) bolded.

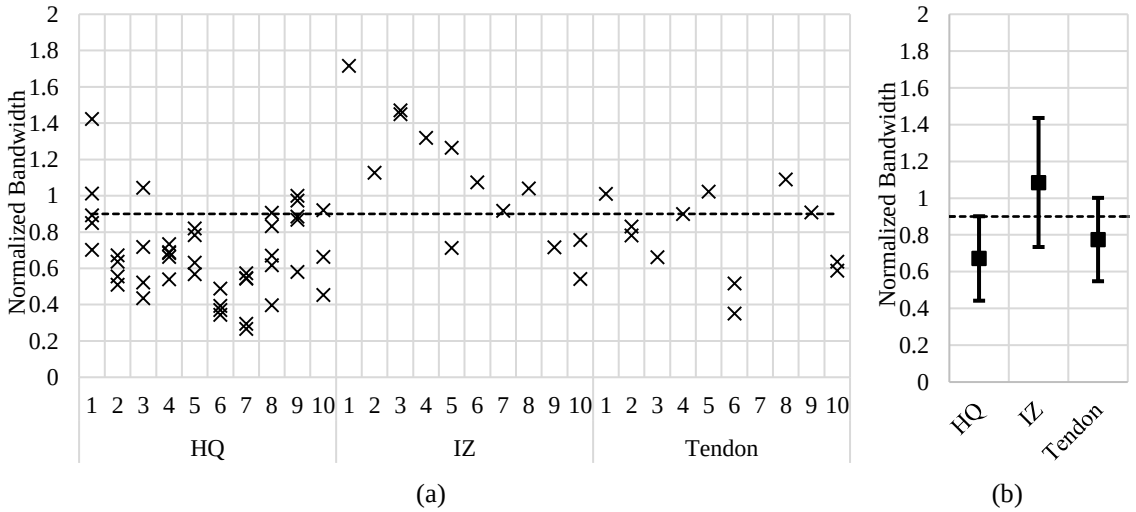

Figure 3-7: a) Scatter plot b) mean and standard deviation of NBW estimates from all subjects grouped by reference channel location.

Table 3-4 delineates KUR values across all subjects and channels. A threshold of 2.4 yielded the best overall classification accuracy at 74.3%. With the threshold set, KUR correctly classified 32 of the 45 (71.1%) HQ channels (>2.4) but 5 out of the 37 (13.5%) classified HQ channels were misclassified (4 of which were channels affected by tendons). Correspondingly, 12 out of 13 (92.3%) LQ channels affected by IZs and 8 out of 12 (66.7%) LQ channels affected by tendons were correctly classified.

Subject	Channel 1	Channel 2	Channel 3	Channel 4	Channel 5	Channel 6	Channel 7
1	1.99	2.25	**2.51**	1.83	2.33	**2.81**	**2.61**
2	2.11	2.29	**2.60**	2.12	**2.57**	**2.78**	2.22
3	**2.44**	**2.61**	**2.47**	2.01	2.24	**2.92**	2.30
4	**2.61**	**2.58**	**2.54**	2.02	**2.47**	**2.45**	2.34
5	2.33	2.16	**2.54**	1.86	2.36	**2.67**	2.39
6	**3.16**	**3.43**	**3.55**	**3.65**	**3.25**	2.12	**3.47**
7	**3.34**	**4.19**	**2.96**	1.90	**3.63**	**3.27**	**2.92**
8	2.27	2.25	**2.54**	2.20	2.06	**2.57**	**2.50**
9	2.39	2.23	2.28	2.18	2.27	**2.61**	2.30
10	**2.71**	**3.03**	**2.52**	**2.68**	2.33	2.17	2.28

Table 3-4: KUR estimates from all subjects and all channels with HQ channels according to expert evaluation marked in grey and HQ channels according to the feature values and the set threshold (>2.4) bolded.

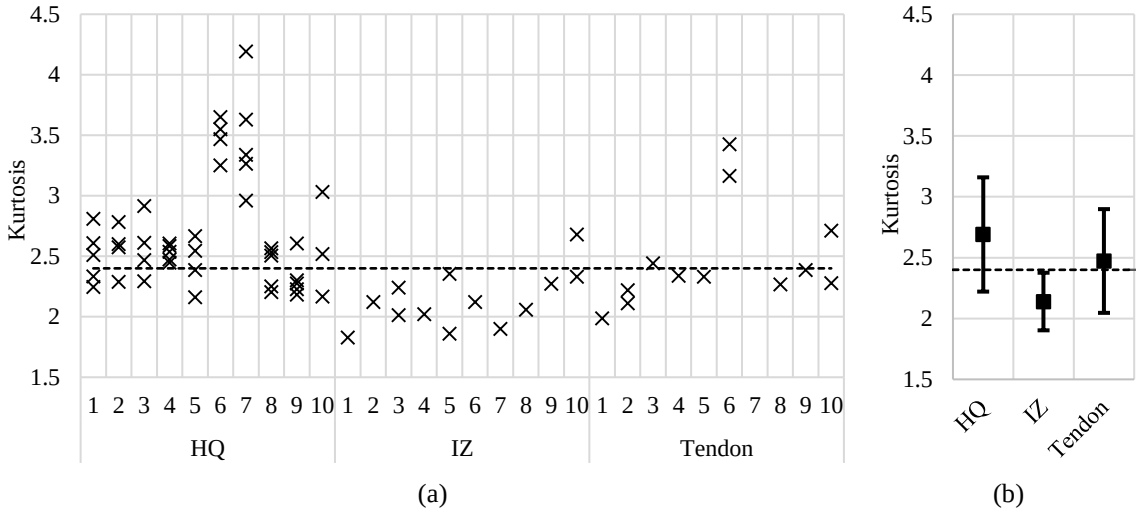

Figure 3-8: a) Scatter plot b) mean and standard deviation of KUR estimates from all subjects grouped by reference channel location.

Table 3-5 delineates BPR values across all subjects and channels. A threshold of 0.15 yielded the best overall classification accuracy at 77.1%. With the threshold set, BPR correctly classified 34 of the 45 (75.6%) HQ channels (<0.15) but 5 out of the 39 (12.8%) classified HQ channels were misclassified (4 of which were channels affected by tendons). Correspondingly, 12 out of 13 (92.3%) LQ channels affected by IZs and 8 out of 12 (66.7%) LQ channels affected by tendons were correctly classified.

Subject	Channel 1	Channel 2	Channel 3	Channel 4	Channel 5	Channel 6	Channel 7
1	0.298	0.166	**0.080**	0.286	0.196	**0.054**	**0.096**
2	0.160	0.236	**0.091**	0.199	0.153	**0.092**	0.260
3	**0.060**	**0.027**	**0.019**	0.169	**0.099**	**0.018**	**0.081**
4	0.177	**0.062**	**0.123**	0.241	**0.079**	**0.064**	0.154
5	0.169	0.240	**0.043**	0.348	0.238	**0.033**	**0.102**
6	**0.077**	**0.043**	**0.072**	**0.033**	**0.097**	0.242	**0.041**
7	**0.087**	**0.025**	**0.106**	0.312	**0.022**	**0.071**	**0.066**
8	**0.078**	**0.096**	**0.023**	**0.129**	0.240	**0.018**	**0.050**
9	0.204	0.272	**0.083**	0.273	0.787	**0.071**	**0.077**
10	0.212	0.168	0.389	0.378	0.633	0.565	0.170

Table 3-5: BPR estimates from all subjects and all channels with HQ channels according to expert evaluation marked in grey and HQ channels according to the feature values and the set threshold (<0.15) bolded.

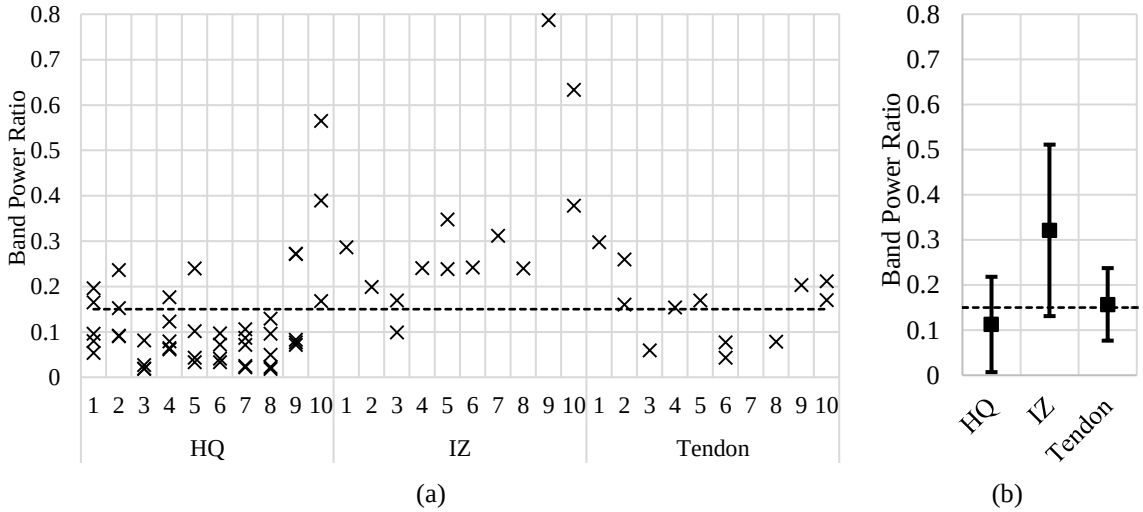

Figure 3-9: a) Scatter plot b) mean and standard deviation of BPR estimates from all subjects grouped by reference channel location.

Table 3-6 delineates AANAP values across all subjects and channels. A threshold of 16 yielded the best overall classification accuracy at 80%. With the threshold set, AANAP correctly classified 36 of the 45 (80%) HQ channels (>16) but 5 out of the 41 classified HQ channels were misclassified (all of which were channels affected by tendons). Correspondingly, 13 out of 13 (100%) LQ channels affected by IZs and 7 out of 12 (58.3%) LQ channels affected by tendons were correctly classified.

Subject	Channel 1	Channel 2	Channel 3	Channel 4	Channel 5	Channel 6	Channel 7
1	14.2	15.9	**16.9**	12.2	14.0	**18.5**	**17.6**
2	15.5	**16.8**	**17.4**	15.5	**16.4**	**17.2**	**16.5**
3	**17.6**	**18.7**	**20.4**	12.4	15.5	**19.0**	**18.0**
4	15.9	**17.6**	**16.6**	14.5	**17.4**	**18.7**	15.9
5	15.1	14.7	**18.2**	13.3	14.1	**19.3**	**16.8**
6	**17.4**	**18.8**	**19.6**	**18.5**	14.0	13.6	**18.6**
7	**17.6**	**20.1**	**17.0**	14.1	**22.1**	**18.5**	**16.5**
8	**17.1**	**17.1**	**19.1**	**18.3**	15.5	**19.5**	**17.5**
9	15.7	**16.2**	**17.5**	14.2	11.8	**18.0**	**16.3**
10	14.8	15.9	13.5	14.5	12.1	13.7	14.9

Table 3-6: AANAP estimates from all subjects and all channels with HQ channels according to expert evaluation marked in grey and HQ channels according to the feature values and the set threshold (>16) bolded.

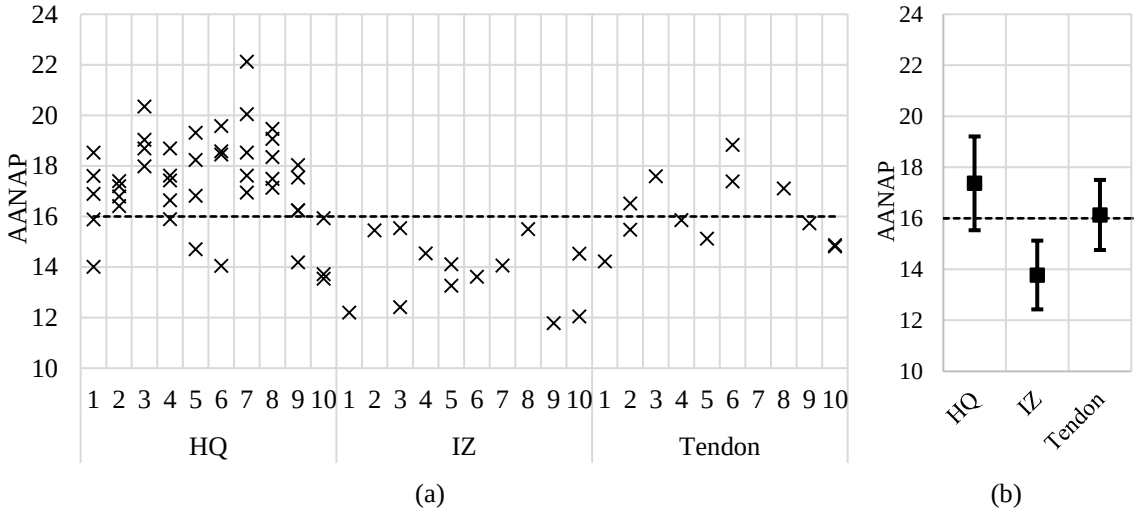

Figure 3-10: a) Scatter plot b) mean and standard deviation of AANAP estimates from all subjects grouped by reference channel location.

Features	Accuracy of Classification					Misclassification Rate of HQ Channels
	Overall	HQ Channels	LQ Channels	IZ-affected	Tendon-affected	
MF	75.7%	73.3%	80%	92.3%	66.7%	13.2%
NBW	72.9%	84.4%	52%	69.2%	33.3%	24.0%
KUR	74.3%	71.1%	80%	92.3%	66.7%	13.5%
BPR	77.1%	75.6%	80%	92.3%	66.7%	12.8%
AANAP	80.0%	80.0%	80%	100%	58.3%	12.2%

Table 3-7: Accuracy of the tested features in classifying electrode location quality and the misclassification rate of HQ channels.

Features	Silhouette Separability		
	HQ to LQ Channels	HQ to IZ-affected	HQ to Tendon-affected
MF	0.251	0.328	0.114
NBW	0.295	0.422	0.047
KUR	0.011	0.043	-0.041
BPR	0.408	0.528	0.099
AANAP	0.249	0.363	0.004

Table 3-8: Silhouette separability of the tested features for different expert evaluated electrode locations.

3.4 Discussion

Based on the results, MF, BPR and AANAP demonstrated better performance when considering accuracy, rate of misclassified HQ channels and silhouette values collectively, compared to NBW and KUR. Specifically, NBW demonstrated a lower accuracy in identifying LQ channels, and as a result yielded a rate of misclassified HQ channels that was almost twice that of MF, BPR or AANAP. Thus, while NBW yielded the highest capacity for identifying HQ channels, it did this at the expense of missing many LQ channels. If NBW was used in practice, it would increase the risk of using LQ channels in analysis compared to other indices, so this feature is not recommended for use as a signal quality index. KUR illustrated low accuracy in classifying HQ channels compared to MF, BPR and AANAP. KUR also has the lowest silhouette value from HQ to LQ channels. As such, KUR would also increase the risk of using LQ channels in analysis compared to other indices, so this feature is also not recommended for use as a signal quality index.

Among the three better-performing features (MF, BPR and AANAP), BPR had the best separability from HQ to LQ channels while AANAP yielded a slightly better accuracy in classifying HQ channels and a slightly lower rate of misclassified HQ channels. All three features yielded high overall classification accuracy and low misclassification rate of HQ channels, indicating that these features have potential as a signal quality index. In this work, when these three feature values indicated a recording as HQ, the recording was actually HQ in over 85% of the cases.

There are a few limitations which suggest proceeding cautiously in recommending MF, BPR and AANAP as signal quality indices. First, all features demonstrated better accuracy and separability for classifying IZ-affected LQ channels compared to tendon-affected ones. Limiting the scope of a signal quality index to detecting IZ-affected areas only, would improve its reliability. It may be prudent therefore, to avoid tendon areas altogether when possible, through judicious placement of electrodes away from the ends of the muscle. Then using a signal quality index, any channels identified within the IZ can be removed from use.

Second, the relatively large interelectrode distance used in this work resulted in a high ratio of channels placed in locations marginally affected by IZ or tendon regions. A smaller electrode spacing and measures for handling marginally-affected channels should allow for more accurate results of expert evaluation and possibly change performances of the evaluated features.

Third, between-subject variability in muscle physiology can cause feature values to also be highly variable, thus reducing the reliability of indices. Even in this small sample size

of 10, one subject (see feature values for Subject 10) stood out among the others, having markedly higher MF values, leading to higher BPR, and lower kurtosis and AANAP. Also, only bicep brachii was tested in this work, a muscle which is known to have well constrained IZ, and relatively parallel fibre structure (Barbero, et al., 2012). Other muscles may have more dispersed IZ, and varying degrees of parallelization, and pennation. All of these factors may make it impossible to identify even a muscle-specific threshold for a reliable signal quality index. Further testing on different muscles and a larger samples size is recommended, and perhaps a more complex fuzzy clustering approach could be used to overcome some of the suggested limitations.

3.5 Conclusions

In this work, five features were tested on MVC recordings collected from 10 subjects using a 7-channel linear electrode array with 20mm interelectrode distance for their ability to classify LQ channels due to proximity to IZs and tendons with simple thresholding. Features MF, BPR and AANAP demonstrated promising results in classifying LQ channels, especially the IZ-affected ones. They may be used to assist in avoiding locations affected by IZs in single-channel SEMG applications by first collecting a 3-second MVC recording from the subject, calculating MF, BPR or AANAP, and comparing the value to the corresponding threshold. Thresholds for each of these features have been established for the biceps brachii in this work; however, further work is warranted to more accurately ascertain these thresholds, to determine the thresholds for other muscles, and in general to verify the reliability of the features as a signal quality index across a more diverse subject pool.

REFERENCES

Barbero, M., Merletti, R. & Rainoldi, A. (2012) *Atlas of Muscle Innervation Zones: Understanding Surface Electromyography and Its Applications*. 1st ed. Milan, Italy: Springer-Verlag Mailand.

Beck, T., Housh, T., Cramer, J., Stout, J., Ryan, E., Herda, T., Costa, P. & Defreitas, J. (2009) 'Electrode placement over the innervation zone affects the low-, not the high-frequency portion of the EMG frequency spectrum'. *Journal of Electromyography and Kinesiology*, August, 19(4), pp. 660-666.

De Luca, C. (2002) *Surface Electromyography: Detection and Recording*, Natick, MA: DelSys.

Farina, D., Merletti, R., Nazzaro, M. & Caruso, I. (2001) 'Effect of joint angle on EMG variables in leg and thigh muscles'. *IEEE Engineering in Medicine and Biology Magazine*, 20(6), pp. 62-71.

Farina, D., Merletti, R. & Stegeman, D. (2004) 'Biophysics of the generation of EMG signals'. In: R. Merletti & P. Parker, eds. *Electromyography: physiology, engineering, and non-invasive applications*. Hoboken: John Wiley & Sons, Inc., pp. 81-105.

Fiori, A. & Zenga, M. (2009) 'Karl Pearson and the Origin of Kurtosis'. *International Statistical Review*, 77(1), pp. 40-50.

Fraser, G., Chan, A., Green, J. & MacIsaac, D. (2014) 'Automated Biosignal Quality Analysis for Electromyography Using a One-Class Support Vector Machine'. *IEEE Transactions on Instrumentation and Measurement*, December, 63(12), pp. 2919-2930.

Gazzoni, M., Afsharipour & Merletti, R. (2016) 'Surface EMG in Ergonomics and Occupational Medicine'. In: R. Merletti & D. Farina, eds. *Surface Electromyography: Physiology, Engineering, and Applications.* Hoboken: John Wiley & Sons, pp. 273-310.

Hug, F. & Tucker, K. (2017) 'Muscle Coordination and the Development of Musculoskeletal Disorders'. *Exercise and Sport Sciences Reviews*, 45(4), pp. 201-208.

Kaufman, L. & Rousseeuw, P. (1990) *Finding Groups in Data: An Introduction to Cluster Analysis*. 1st ed. Hoboken, New Jersey: John Wiley & Sons.

Komi, P. & Viitasalo, J. (1975) 'Signal characteristics of EMG with special reference to reproducibility of measurements'. *Acta physiologica Scandinavica*, Volume 93, pp. 531-539.

Lang, A.H., Nurkkanen, P., Vaahtoranta, K.M. (1971) 'Automatic sampling and averaging of electromyographic unit potentials'. *Electroencephalography and Clinical Neurophysiology*, 31, pp. 404-406.

Masuda, T., Miyano, H. & Sadoyama, T. (1985) 'A surface electrode array for detecting action potential trains of single motor units'. *Electroencephalography and Clinical Neurophysiology*, May, 60(5), pp. 435-443.

Merletti, R., Farina, D. & Gazzoni, M. (2003) 'The linear electrode array: a useful tool with many applications'. *Journal of Electromyography and Kinesiology*, February, 13(1), pp. 37-47.

Merletti, R., Farina, D. & Granata, A. (1999) 'Non-invasive assessment of motor unit properties with linear electrode arrays'. *Electroencephalography and Clinical Neurophysiology*, 50(supplementary), pp. 293-300.

Merletti, R., Merlo, A. & Rainoldi, A. (2001a) 'Electrode placement in dynamic surface EMG: the effect of innervation zone'. *ESMAC & SIAMOC Joint Congress*, 12-14 October, 14(2), p. 120.

Merletti, R., Rainoldi, A. & Farina, D. (2001b) 'Surface EMG for non-invasive muscle Characterization'. *Exercise and Sport Sciences Reviews*, 29(1), pp. 20-25.

Merlo, A. & Campanini, I. (2016) 'Applications in Movement and Gait Analysis'. In: R. Merletti & D. Farina, eds. *Surface Electromyography: Physiology, Engineering, and Applications.* Hoboken: John Wiley & Sons, pp. 273-310.

Naik, G.R., Easter Selvan, S. & Nguyen, H.T. (2016) 'Single-Channel EMG Classification With Ensemble-Empirical-Mode-Decomposition-Based ICA for Diagnosing Neuromuscular Disorders'. *IEEE Transactions on Neural Systems and Rehabilitation Engineering*, 24(7), pp. 734-743.

Rainoldi, A., Melchiorri, G. & Caruso, I. (2004) 'A method for positioning electrodes during surface EMG recordings in lower limb muscles'. *Journal of Neuroscience Methods*, Volume 134, p. 37–43.

Rainoldi, A., Nazzaro, M., Merletti, R., Farina, D., Caruso, I. & Gaudenti, S. (2000) 'Geometrical factors in surface EMG of the vastus medialis and lateralis muscles'. *Journal of Electromyography and Kinesiology*, Volume 10, p. 327–336.

Roy, S., De Luca, C. & Schneider, J. (1986) 'Effects of electrode location on myoelectric conduction velocity and median frequency estimates'. *Journal of Applied Physiology*, 61(4), pp. 1510-1517.

Sturma, A., Hruby, L.A., Prahm, C., Mayer, J.A. & Aszmann, O.C. (2018) 'Rehabilitation of Upper Extremity Nerve Injuries Using Surface EMG Biofeedback: Protocols for Clinical Application'. Frontiers in Neuroscience, 12, pp. 906.

von Tscharner, V. (2000) 'Intensity analysis in time-frequency space of surface myoelectric signals by wavelets of specified resolution'. *Journal of Electromyography and Kinesiology*, 10(6), pp. 433-445.

Westfall, P. (2014) 'Kurtosis as Peakedness, 1905-2014. R.I.P.'. *The American Statistician*, 68(3), pp. 191-195.

CHAPTER 4 CONCLUSION

The primary purpose of this work was to provide insight into the variability of SEMG features. In particular, MF and MAV were examined and their baseline, within-trial, and between-trial variability was reported using CoV. Then variability across electrode locations and subjects was examined for a variety of features, with the aim to identify a feature whose variability across location could be exploited to avoid low quality measurements resulting from poorly-positioned electrodes.

Given the purpose of this work, the first objective was to establish baseline variability in MF and MAV due solely to sampling error. With all sources of variability controlled in simulation, the baseline variability for 1-second segments was 2.96% for MF and 4.40% for MAV. These values provide guidance for what to expect in measurements for stationary SEMG signals. Any observed variability higher than these values indicates the existence of non-stationarities in the signals being measured. However, it is important to remember that baseline variability decreases as segment length increases.

During the generation of SEMG signals, the physiological parameters associated with the corresponding muscle have influence on feature values. The second objective of this work was to determine the significance of parameter influence on MF and MAV through a sensitivity analysis conducted in simulation. Results of the sensitivity analysis indicate that both MF and MAV are considerably affected by changes in average fibre depth and conduction velocity, in a way that both features decrease when fibre depth increases and increase when conduction velocity increases. MAV also increases with increasing number of motor units while MF does not. This kind of sensitivity analysis can be applied

to any SEMG feature and is useful in helping to explain higher-than-baseline variability observed in measurements.

The third objective for this work was to infer the varying physiological parameters present during two *in vivo* protocols – within-trial and between-trial tests – using information gained from achieving objectives 1 and 2. During the within-trial test that represented an attempt to match simulation conditions, variability in MF (3.18%) was similar to its baseline value, while variability in MAV (12.00%) was much higher than its baseline value. The higher-than-baseline variability in MAV is an interesting result, given that the activity protocol used to elicit contractions during measurement ensured that subjects remained stationary (joint angle varied less than 1 degree) while holding a movable weight, thus ensuring constant force and position. These are the conditions generally accepted in SEMG analysis to ensure stationarity in the signals being measured, yet the results from this work indicate that this assertion may not be completely valid. This could be a significant finding for experimentation when stationarity in the signal is important. The fact that MAV was affected but MF was not, suggests that constant-force, constant-position contractions are driven by a recruitment pattern which charges and discharges a variable number of motor units, but from a pool of units with similar depths and CVs. The between-trial test introduced the effect of restarting a contraction from rest. Under these conditions variability increased in both MF and MAV compared to baseline and even compared to within-trial values (to 4.08% and 14.83% respectively). Since both variables indicated higher-than-baseline values under these conditions, it is likely that contractions which start from rest are not constrained to recruit units from a pool with similar depths and/or CVs. The findings related to objective 3 provide useful

insights to future studies that use SEMG features. For example, for studies that track muscle state with SEMG features, such as tracking fatigue with MF or tracking force with MAV (Merletti, et al., 2016), the reported variability in this work provides guidance for what to expect in measurements even when the state of interest is not changing.

Reported findings can also be used to improve simulation models like the one used in this work. The current version of MyoSim does not account for variable recruitment during a contraction, nor does it allow user control of recruitment patterns beyond specifying ranges for random selection of motor units. The reported variability values and the observed sensitivities from this work could be used to build in recruitment schemes which more accurately model within-trial and between-trial conditions. This could have significant impact on analysis strategies which compare simulated and measured data sets, like the one proposed by Phillips (2016), which attempted to compare measured data with simulated data as a way to check for noise contamination.

A few limitations exist in the achievement of objectives 1 through 3. First, only two features (MF and MAV) and two contraction levels (15% and 25% MVC) were included in the analysis. More features and more contractions levels should be investigated in future work to obtain more generalized results. Providing the kind of information presented in this work for additional features could have the added benefit of narrowing in on physiological changes during measurement, since different features may exhibit different sensitivity profiles. Also, this work reported on 1-second segments, but showed that variability is segment-length-dependent. Since many control strategies aim to use very short segment lengths (160ms) (Robertson, et al., 2018), re-analysis at lengths in this order might be useful.

The fourth objective for this work was to search for a SEMG feature that could clearly separate data collected from electrode locations close to IZs and tendon regions (low-quality locations) from data collected away from those regions (high-quality locations). To establish a separation threshold that would be valid for all subjects, variability in the feature across locations would have to be sufficiently greater than variability across subjects. Three features demonstrated promising performance by correctly identifying >80% of all low-quality locations, and >90% of IZ-affected low-quality locations. These features were MF, BPR, and AANAP with threshold values set to 70Hz, 0.15 and 16 respectively.

The findings related to objective 4 can provide guidance for placing electrodes in a high quality location during SEMG measurement when only a single channel is available. However, more work should be done to validate the reliability of the reported thresholds, and the utility of the approach more generally. To do so, a larger subject pool should be observed, along with different muscle groups. It is likely that utility will be restricted to muscles with a high degree of fibre parallelization (low pennation). Finally, it is recommended that in future studies, an inter-electrode distance less than 5mm is used, to improve spatial resolution between high-quality and low-quality locations

The results of this work provide researchers and clinicians with additional understanding about SEMG feature variability and guidance for what to expect under baseline, within-trial and between-trial conditions. This can be useful for setting up SEMG measurement devices or for tuning SEMG-based assistive devices. The work also provides insight into factors contributing to the variability in each of these conditions, in hopes to enable better data interpretation and/or data acquisition protocol designs.

REFERENCES

Al-Angari, H., Kanitz, G., Tarantino, S. & Cipriani, C. (2016) 'Distance and mutual information methods for EMG feature and channel subset selection for classification of hand movements'. *Biomedical Signal Processing and Control,* Volume 27, pp. 24-31.

Araujo, R., Duarte, M. & Amadio, A. (2000) 'On the inter- and intra-subject variability of the electromyographic signal in isometric contractions'. *Electromyography and Clinical Neurophysiology,* 40(4), pp. 225-229.

Arjunan, S., Kumar, D.K. & Naik, G. (2014) 'Computation and Evaluation of Features of Surface Electromyogram to Identify the Force of Muscle Contraction and Muscle Fatigue'. *BioMed Research International,* p. 6 pages.

Balshaw, T., Fry, A., Maden-Wilkinson, T.M., Kong, P.W. & Folland, J.P. (2017) 'Reliability of quadriceps surface electromyography measurements is improved by two vs. single site recordings'. *European Journal of Applied Physiology,* 117(6), pp. 1085-1094.

Baratta, R.V., Solomonow, M., Zhou, B. & Zhu, M. (1998) 'Methods to reduce the variability of EMG power spectrum estimates'. *Journal of Electromyography and Kinesiology,* 8(5), pp. 279-285.

Carius, D., Kugler, P., Kuhwald, H.M. & Wollny, R. (2015) 'Absolute and relative intrasession reliability of surface EMG variables for voluntary precise forearm movements'. *Journal of Electromyography and Kinesiology,* 25(6), pp. 860-869.

Chan, A.D.C., no date. *Matlab Library - Adrian D.C. Chan Homepage* [Online]. Available at: http://www.sce.carleton.ca/faculty/chan/index.php?page=matlab (Accessed: 6 November 2018).

De Luca, C. (1984) 'Myoelectrical manifestations of localized muscular fatigue in humans'. *Critical Reviews in Biomedical Engineering,* 11(4), pp. 251-279.

Du, Y., Jin, W., Wei, W., Hu, Y. & Geng, W. (2017) 'Surface EMG-Based Inter-Session Gesture Recognition Enhanced by Deep Domain Adaptation'. *Sensors (Basel),* 17(3), p. 458.

Ebenbichler, G.R., Bonato, P., Roy, S.H., Lehr, S., Posch, M., Kollmitzer, J. & Della Croce, U. (2002) 'Reliability of EMG time-frequency measures of fatigue during repetitive lifting'. *Medicine & Science in Sports & Exercise,* 34(8), pp. 1316-1323.

Englehart, K. & Hudgins, B. (2003) 'A robust, real-time control scheme for multifunction myoelectric control'. *IEEE Transactions on Biomedical Engineering,* 50(7), pp. 848-854.

Farina, D., Merletti, R. & Enoka, R.M. (2004) 'The extraction of neural strategies from the surface EMG'. *Journal of Applied Physiology,* 96(4), pp. 1486-1495.

Gazzoni, M., Afsharipour & Merletti, R. (2016) ‘Surface EMG in Ergonomics and Occupational Medicine’. In: R. Merletti & D. Farina, eds. *Surface Electromyography: Physiology, Engineering, and Applications.* Hoboken: John Wiley & Sons, pp. 273-310.

Gross, D., Grassino, A., Ross, W.R. & Macklem, P.T. (1979) ‘Electromyogram pattern of diaphragmatic fatigue’. *Journal of Applied Physiology: Respiratory, Environmental and Exercise Physiology,* 46(1), pp. 1-7.

Hermens, H.J. & Freriks, B. (1997) *SENIAM 5: The State of the Art on Sensors and Sensor Placement Procedures for Surface ElectroMyoGraphy: A proposal for sensor placement procedures*, Enschede: Roessingh Research and Development.

Hudgins, B., Parker, P. & Scott, R.N. (1993) ‘A New Strategy for Multifunction Myoelectric Control’. *IEEE Transactions on Biomedical Engineering,* 40(1), pp. 82-94.

Hug, F. & Tucker, K. (2017) ‘Muscle Coordination and the Development of Musculoskeletal Disorders’. *Exercise and Sport Sciences Reviews*, 45(4), pp. 201-208.

Jensen, C., Vasseljen, O. & Westgaard, R.H. (1993a) ‘The influence of electrode position on bipolar surface electromyogram recordings of the upper trapezius muscle’. *European Journal of Applied Physiology*, 67(3), pp. 266-273.

Jensen, R., Fuglsang-Frederiksen, A. & Olesen, J. (1993b) ‘Quantitative surface EMG of pericranial muscles. Reproducibility and variability’. *Electroencephalography and Clinical Neurophysiology/Evoked Potentials Section,* 89(1), pp. 1-9.

Karamanidis, K., Arampatzis, A. & Brüggemann, G. (2002) ‘Reproducibility of electromyographic and dynamic parameters during running on a treadmill with deliberate changes in running technique’. *Deutsche Zeitschrift fur Sportmedizin,* 53(4), pp. 107-113.

Kollmitzer, J., Ebenbichler, G.R. & Kopf, A. (1999) ‘Reliability of surface electromyographic measurements’. *Clinical Neurophysiology,* 110(4), pp. 725-734.

Komi, P.V. & Viitasalo, J.H. (1976) ‘Signal Characteristics of EMG at Different Levels of Muscle Tension’. *Acta Physiologica,* 96(2), pp. 267-276.

MacIsaac, D. (2004) ‘A Robust Index of Localized Muscle Fatigue’, PhD Thesis, University of New Brunswick, Fredericton, Canada.

MacIsaac, D., Rogers, D. & Bhandarkar, A. (2006) ‘Simulating Myoelectric Signals with a Finite-Length Model of Muscle’. *Proceedings of the 29th Conference of the Canadian Medical and Biological Engineering Society*. Vancouver, Canada.

MacIsaac, D., Tallam Puranam Raghu, S. & Shi, Y. (2018) ‘MyoSim 2.0: Enhancing and Validating an EMG Simulation Tool’. *Proceedings of the 41st Conference of the Canadian Medical and Biological Engineering Society*. Charlottetown, PEI, Canada.

Marco, G., Alberto, B. & Taian, V. (2017) ‘Surface EMG and muscle fatigue: multi-channel approaches to the study of myoelectric manifestations of muscle fatigue’. *Physiological Measurement,* 38(5), pp. R27-R60.

McCarthy, C.J., Callaghan, M.J. & Oldham, J.A. (2008) 'The reliability of isometric strength and fatigue measures in patients'. *Manual Therapy,* 13(2), pp. 159-164.

Merletti, R., Afsharipour, B., Dideriksen, J. & Farina, D. (2016) 'Muscle Force and Myoelectric Manifestations of Muscle Fatigue in Voluntary and Electrically Elicited Contractions'. In: R. Merletti & D. Farina, eds. *Surface Electromyography: Physiology, Engineering, and Applications.* Hoboken: John Wiley & Sons, pp. 273-310.

Merletti, R., Farina, D. & Gazzoni, M. (2003) 'The linear electrode array: a useful tool with many applications'. *Journal of Electromyography and Kinesiology,* February, 13(1), pp. 37-47.

Merletti, R., Rainoldi, A. & Farina, D. (2001) 'Surface Electromyography for Noninvasive Characterization of Muscle'. *Exercise & Sport Sciences Reviews,* January, 29(1), pp. 20-25.

Merlo, A. & Campanini, I. (2016) 'Applications in Movement and Gait Analysis'. In: R. Merletti & D. Farina, eds. *Surface Electromyography: Physiology, Engineering, and Applications.* Hoboken: John Wiley & Sons, pp. 273-310.

Naik, G.R., Easter Selvan, S. & Nguyen, H.T. (2016) 'Single-Channel EMG Classification With Ensemble-Empirical-Mode-Decomposition-Based ICA for Diagnosing Neuromuscular Disorders'. *IEEE Transactions on Neural Systems and Rehabilitation Engineering,* 24(7), pp. 734-743.

Natus Medical Inc. (©2016). '*Nicolet EDX Synergy NCS / EMG / EP / IOM System Product Page*'. San Carlos, CA: Natus Medical Inc. P/N 021173A. [Viewed 17 December 2019]. Available from: https://partners.natus.com/asset/resource/file/neuro/asset/2018-04/021173A%20Synergy%20on%20EDX%20page%20fnl.pdf

Nazarpour, K., Al-Timemy, A.H., Bugmann, G. & Jackson, A. (2013) 'A note on the probability distribution function of the surface electromyogram signal'. *Brain Research Bulletin,* Volume 90, pp. 88-91.

Ng, J. & Richardson, C. (1996) 'Reliability of electromyographic power spectral analysis of back muscle endurance in healthy subjects'. *Archives of Physical Medicine and Rehabilitation,* 77(3), pp. 259-263.

Oskoei, M.A. & Hu, H. (2008) 'Support Vector Machine-Based Classification Scheme for Myoelectric Control Applied to Upper Limb'. *IEEE Transactions on Biomedical Engineering,* 55(8), pp. 1956-1965.

Phillips, G. (2016) 'Pairwise Attribute Noise Detection Algorithm for Detecting Noise in Surface Electromyography Recordings', MScE Thesis, University of New Brunswick, Fredericton, Canada.

Phinyomark, A. Thongpanja, S., Hu, H., Phukpattaranont, P. & Limsakul, C. (2012) 'The Usefulness of Mean and Median Frequencies in Electromyography Analysis'. In: G. R.

Naik, ed. *Computational Intelligence in Electromyography Analysis.* s.l.:IntechOpen, pp. 195-220.

Piccoli, M., Rainoldi, A., Heitz, C., Wüthrich, M., Boccia, G., Tomasoni, E., Spirolazzi, C., Egloff, M. & Barbero, M. (2014) 'Innervation zone locations in 43 superficial muscles: toward a standardization of electrode positioning'. *Muscle & Nerve*, 49(3), pp. 413-421.

Plonsey, R. (1974) 'The active fiber in a volume conductor'. *IEEE Transactions on Biomedical Engineering*, Sept., 21(5), pp. 371-381.

Rainoldi, A., Galardi, G., Maderna, L., Comi, G., Lo Conte, L. & Merletti, R. (1999) 'Repeatability of surface EMG variables during voluntary isometric contractions of the biceps brachii muscle'. *Journal of Electromyography and Kinesiology*, 9(2), pp. 105-119.

Rainoldi, A., Melchiorri, G. & Caruso, I. (2004) 'A method for positioning electrodes during surface EMG recordings in lower limb muscles'. *Journal of Neuroscience Methods*, 15 March, 134(1), pp. 37-43.

Robertson, J.W., Englehart, K.B. & Scheme, E.J. (2018) 'Rejection of Systemic and Operator Errors in a Real-Time Myoelectric Control Task'. *Proceedings of 40th Annual International Conference of the IEEE Engineering in Medicine and Biology Society (EMBC).* Honolulu, HI.

Rogers, D.R. & MacIsaac, D.T. (2011) 'EMG-based muscle fatigue assessment during dynamic contractions using principal component analysis'. *Journal of Electromyography and Kinesiology*, 21(5), pp. 811-818.

Rogers, D.R. & MacIsaac, D.T. (2013) 'A comparison of EMG-based muscle fatigue assessments during dynamic contractions'. *Journal of Electromyography and Kinesiology*, 23(5), pp. 1004-1011.

Roy, S.H., De Luca, C.J. & Schneider, J. (1986) 'Effects of electrode location on myoelectric conduction velocity and median frequency estimates'. *Journal of Applied Physiology*, 61(4), pp. 1510-1517.

Scheme, E. & Englehart, K. (2014) 'On the robustness of EMG features for pattern recognition based myoelectric control: A multi-dataset comparison'. *Proceedings of 36th Annual International Conference of the IEEE Engineering in Medicine and Biology Society.* Chicago, IL, USA.

Smith, L.H., Hargrove, L.J., Lock, B.A. & Kuiken, T.A. (2010) 'Determining the Optimal Window Length for Pattern Recognition-Based Myoelectric Control: Balancing the Competing Effects of Classification Error and Controller Delay'. *IEEE Transactions on Neural Systems and Rehabilitation Engineering*, 19(2), pp. 186-192.

Sorbie, G.G., Williams, M.J., Boyle, D.W., Gray, A., Brouner, J., Gibson, N., Baker, J.S., Easton, C. & Ugbolue, U.C. (2018) 'Intra-session and Inter-day Reliability of the Myon

320 Electromyography System During Sub-maximal Contractions'. *Frontiers in Physiology*, 9(309), p. 7 pages.

Sturma, A., Hruby, L.A., Prahm, C., Mayer, J.A. & Aszmann, O.C. (2018) 'Rehabilitation of Upper Extremity Nerve Injuries Using Surface EMG Biofeedback: Protocols for Clinical Application'. Frontiers in Neuroscience, 12, pp. 906.

Zaman, S. (2012) 'Repeatability in EMG-based Muscle Fatigue Assessment Strategies',: MScE Thesis, University of New Brunswick, Fredericton, Canada.

APPENDIX A: Detailed Results for Chapter 2

The mean, standard deviation (SD) and coefficient of variation (CoV) presented below were calculated across quantity values estimated from 1-second segments of a specific recording. Recall that the theoretical CoV (T. CoV) of MAV of a recording is calculated using Equation 2-4 based on the statistical bandwidth B_S estimated from the recording while the CoV is the ratio of SD to mean across the 1-second segments of the recording. The conduction velocity (CV) estimates were obtained using the time delay of the maximum cross-correlation and the inter-electrode distance. The SD of elbow angle was obtained from elbow angle values recorded by a potentiometer that turned with the disc apparatus used to perform the tests.

A.1. Results from Simulated Data

Each simulated data is 100 second in length, resulting in 100 1-second segments and thus 100 estimates for each quantity. These 22 recordings were simulated with CV, average fibre depth NMU and fibre geometry varied to have their PSD (power spectral density) estimates matched with those of the within-trial records, at an energy-normalized mean absolute error of 7.5×10^{-3} or less.

Records		Mean Frequency			Mean Absolute Value			
MVC matched	Subject matched	Mean (Hz)	SD	CoV (%)	Mean (μV)	SD	CoV (%)	T. CoV (%)
25%	1	78.07	2.36	3.03	76.91	3.65	4.75	4.64
	2	76.41	2.32	3.03	141.42	5.88	4.16	4.67
	3	74.52	2.21	2.97	82.69	3.23	3.91	4.91
	4	86.18	2.35	2.73	92.54	4.55	4.91	4.52
	5	94.16	2.15	2.29	119.86	5.57	4.65	4.32
	6	67.54	2.33	3.45	27.00	1.23	4.57	5.05
	7	74.07	2.31	3.12	90.84	4.10	4.52	4.79
	8	77.58	2.78	3.58	39.57	1.77	4.48	4.72
	9	78.60	2.07	2.64	54.99	2.60	4.74	4.70
	10	76.37	2.40	3.14	32.74	1.42	4.32	4.67
	11	85.34	2.13	2.49	80.71	3.47	4.29	4.50
15%	1	82.37	2.31	2.80	42.63	2.00	4.69	4.60
	2	79.31	2.66	3.36	68.41	3.06	4.47	4.70
	3	73.00	2.24	3.06	57.77	2.58	4.46	4.86
	4	87.37	2.26	2.58	62.21	2.66	4.27	4.48
	5	88.56	2.56	2.89	62.24	2.77	4.46	4.45
	6	64.11	2.27	3.55	14.84	0.67	4.55	5.17
	7	75.38	2.33	3.09	25.15	1.18	4.69	4.80
	8	85.71	2.32	2.70	22.25	0.91	4.09	4.46
	9	83.26	2.37	2.85	27.90	1.08	3.87	4.55
	10	84.62	2.21	2.61	24.62	0.90	3.66	4.45
	11	75.51	2.38	3.16	25.95	1.09	4.19	4.75
Average across records		79.46	2.33	2.96	57.87	2.56	4.40	4.67
SD across records		7.10	0.16	0.34	33.90	1.52	0.32	0.21

A.2. Results from Within-trial Records

Each within-trial record is 15 seconds in length, resulting in 15 1-second segments and thus 15 estimates for each quantity. Each of these 22 records was collected from the bicep brachii muscle during a single isometric/isotonic contraction at 15% or 25% MVC.

Subject	MVC (lb)	Load	MF		MAV		CV		SD of Elbow Angle
			Mean (Hz)	CoV (%)	Mean (μV)	CoV (%)	Mean (m/s)	CoV (%)	(degree)
1	33	8	78.6	2.30	83.1	20.16	6.25	5.09	1.79
		4.5	78.6	3.01	43.6	14.32	5.56	7.39	0.23
2	25	5	78.7	3.32	134.1	9.71	7.14	6.34	0.20
		3.5	79.5	2.76	79.1	11.26	5.56	9.53	0.59
3	27	6.5	69.4	4.12	80.9	10.16	4.17	4.50	0.14
		4	70.7	2.92	55.4	7.30	3.85	4.22	0.12
4	48	12	85.4	3.62	88.7	23.47	4.17	2.12	0.21
		7	87.9	2.30	66.4	9.44	4.17	2.21	0.38
5	37	9	92.9	2.97	119.3	16.54	5.00	5.09	0.71
		5.5	92.7	3.98	65.6	20.23	4.55	4.88	0.54
6	37	9	68.5	3.03	26.1	10.59	4.55	5.52	0.11
		5.5	68.5	3.25	13.2	5.54	4.17	7.47	0.08
7	30	7.5	73.8	3.85	93.6	13.27	4.17	2.71	0.14
		4.5	73.4	3.04	26.9	10.94	4.55	7.70	0.11
8	40	10	80.4	2.40	42.4	8.59	5.00	6.63	0.91
		6	82.8	2.80	22.4	6.85	4.55	3.45	0.26
9	40	10	79.7	2.61	54.5	17.10	5.56	3.52	0.39
		6	87.9	2.46	25.0	10.00	5.56	6.34	0.72
10	40	10	75.5	5.99	35.4	13.20	4.42	9.05	0.85
		6	86.9	3.21	25.7	10.51	5.00	9.31	0.11
11	36	8	84.0	2.86	88.9	6.64	5.05	5.35	0.08
		4.5	80.1	3.17	23.3	8.08	5.21	7.66	0.12
Mean across records			79.8	3.18	58.8	12.00	5.02	5.82	0.37
SD across records			7.3	0.81	33.8	4.84	0.85	2.15	0.40

A.3. Results from Between-trial Records

Each within-trial record is 15 second in length, resulting in 15 1-second segments and thus 15 estimates for each quantity. Each of these 22 records contains 15 1-second segments, which were extracted from the middle of 15 5-second isometric/isotonic contractions in the same session, with 60-second rests enforced between contractions, from the bicep brachii muscle, at 15% or 25% MVC.

Subject	MVC (lb)	Load (lb)	MF Mean (Hz)	MF CoV (%)	MAV Mean (μV)	MAV CoV (%)	CV Mean (m/s)	CV CoV (%)	SD of Elbow Angle (degree)
1	33	8	96.5	2.37	31.0	12.71	8.33	7.20	2.76
		4.5	104.6	4.48	23.9	12.94	4.55	113.46	2.80
2	25	5	75.9	4.43	143.9	12.57	7.14	16.27	0.15
		3.5	74.1	4.03	95.7	17.29	5.56	9.91	0.59
3	27	6.5	67.1	4.61	61.6	11.97	7.14	26.34	1.39
		4	74.3	4.16	40.7	27.02	3.57	4.23	0.12
4	48	12	82.8	4.74	107.2	11.09	4.55	4.05	0.52
		7	88.8	4.21	56.5	12.08	4.35	3.80	0.42
5	37	9	96.3	4.41	116.9	16.66	5.56	11.15	0.71
		5.5	93.0	3.72	68.9	27.02	5.00	21.76	0.87
6	37	9	71.5	3.16	25.0	12.87	4.55	4.11	0.15
		5.5	71.5	2.93	21.0	7.76	4.17	4.61	0.19
7	30	7.5	75.0	3.99	61.9	10.55	4.17	6.64	0.14
		4.5	70.9	5.84	29.2	15.03	3.85	7.78	0.21
8	40	10	81.3	4.24	51.0	12.74	8.33	16.18	0.41
		6	81.6	4.51	26.3	18.38	3.85	80.82	0.71
9	40	10	79.2	8.17	75.4	32.23	3.57	8.01	0.77
		6	74.1	10.75	23.3	29.46	3.33	44.24	0.72
10	40	10	93.2	7.34	35.4	13.20	5.00	11.23	1.85
		6	90.0	4.44	25.7	10.51	5.56	8.96	1.58
11	36	8	84.8	3.85	81.8	12.91	4.55	6.31	0.39
		4.5	80.8	4.23	41.0	10.93	4.55	5.63	0.25
Mean across records			80.9	4.67	59.2	15.66	5.01	17.96	0.82
SD across records			10.5	1.79	35.4	6.66	1.40	26.50	0.76

Curriculum Vitae

Candidate's Full Name: Yiyang Shi

Universities Attended Xi'an Jiaotong-Liverpool University, Bachelor of Engineering in Electrical Engineering (Honours), 2009-2013

Publications:

1. Shi, Y., MacIsaac, D. M. & Parker, P. A., 2019. Within-trial and Between-trial Variability in Surface EMG Features. *Journal of Electromyography and Kinesiology* (Submitted).

2. Shi, Y., MacIsaac, D. M., Chan, A. D. C. & Parker, P. A., 2019. A Signal Quality Index for Electrode Location Using Single-channel Serface EMG Features. *Journal of Electromyography and Kinesiology* (Submitted).

Conference Presentations:

1. Shi, Y., MacIsaac, D. M. & Parker, P. A., "Variability of Features Extracted from SEMG Signal," *Proceedings of XX International Society of Electrophysiology and Kinesiology Congress*, Chicago, USA, 2016